

Review

# Noncovalent Bonds through Sigma and Pi-Hole Located on the Same Molecule. Guiding Principles and Comparisons

Wiktor Zierkiewicz <sup>1,\*</sup>, Mariusz Michalczyk <sup>1,\*</sup> and Steve Scheiner <sup>2</sup>

<sup>1</sup> Faculty of Chemistry, Wrocław University of Science and Technology, Wybrzeże Wyspiańskiego 27, 50-370 Wrocław, Poland

<sup>2</sup> Department of Chemistry and Biochemistry, Utah State University Logan, Logan, UT 84322-0300, USA; steve.scheiner@usu.edu

\* Correspondence: wiktoria.zierkiewicz@pwr.edu.pl (W.Z.); mariusz.michalczyk@pwr.edu.pl (M.M.)

**Abstract:** Over the last years, scientific interest in noncovalent interactions based on the presence of electron-depleted regions called  $\sigma$ -holes or  $\pi$ -holes has markedly accelerated. Their high directionality and strength, comparable to hydrogen bonds, has been documented in many fields of modern chemistry. The current review gathers and digests recent results concerning these bonds, with a focus on those systems where both  $\sigma$  and  $\pi$ -holes are present on the same molecule. The underlying principles guiding the bonding in both sorts of interactions are discussed, and the trends that emerge from recent work offer a guide as to how one might design systems that allow multiple noncovalent bonds to occur simultaneously, or that prefer one bond type over another.

**Keywords:** molecular electrostatic potential; halogen bond; pnictogen bond; tetrel bond; chalcogen bond; cooperativity



**Citation:** Zierkiewicz, W.; Michalczyk, M.; Scheiner, S. Noncovalent Bonds through Sigma and Pi-Hole Located on the Same Molecule. Guiding Principles and Comparisons. *Molecules* **2021**, *26*, 1740. <https://doi.org/10.3390/molecules26061740>

Academic Editor: Teobald Kupka

Received: 5 March 2021

Accepted: 17 March 2021

Published: 20 March 2021

**Publisher's Note:** MDPI stays neutral with regard to jurisdictional claims in published maps and institutional affiliations.



**Copyright:** © 2021 by the authors. Licensee MDPI, Basel, Switzerland. This article is an open access article distributed under the terms and conditions of the Creative Commons Attribution (CC BY) license (<https://creativecommons.org/licenses/by/4.0/>).

## 1. Introduction

The concept of the  $\sigma$ -hole, introduced to a wide audience in 2005 at a conference in Prague by Tim Clark [1], influenced a way of thinking about noncovalent interactions that prevails to this day. Early experimental findings [2–5] of unusual halogen-halogen contacts were explained in part by the anisotropic distribution of electronic density around a halogen atom when linked to an electron-withdrawing group. Already in 1992, it had been learned that electronegative atoms from Groups 14–17 have regions of positive molecular electrostatic potential (MEP) on their outer surfaces, along an extension of a covalent bond, which may attract an incoming Lewis base [6]. This observation led to the further computational studies which resulted in formulation of the  $\sigma$ -hole idea [7] which was further generalized in later works [7–17]. These ideas concerning the halogen bond were successfully adapted to atoms from other families of the periodic table, which were later grouped into the category of  $\sigma$ -hole bonds. This general sort of noncovalent bond has been subdivided by the specific family from which the bridging atom is drawn, i.e., chalcogen [18–23], pnictogen (pnictogen) [24–28], or tetrel bonds [29–31]. The former, along with the halogen bond, has been formally recognized and detailed in recent IUPAC recommendations [32,33].

Quite the opposite from representing exotic or unusual contacts, these bonds make important contributions to numerous fields of chemistry and biology. As examples, understanding the forces behind crystal engineering and supramolecular chemistry benefits from a knowledge of  $\sigma$ -hole interactions due to their directionality, strength, and self-organization properties which promote formation of adducts in the solid state [34–52]. The importance of  $\sigma$ -hole bonding has also been verified in the context of anion recognition processes [53–61], materials chemistry [62–72], or biochemistry [73–81]. An early work connecting  $\sigma$ -hole bonds with crucial concepts in chemistry occurred when Grabowski

recognized that tetrel bonds can be thought of as a preliminary stage of the very important  $S_N2$  reaction [82].

As ideas concerning the  $\sigma$ -hole were proliferating, it was recognized that density depletion is not necessarily limited only to the extensions of covalent bonds. Depletions can also occur above planar groups as well, as for example above a carbonyl or phenyl group. Linear systems such as HCN can also suffer from low density off the molecular axis. Because of their location and association with  $\pi$ -electronic systems, these regions of density depletion and positive electrostatic potential have come to be called  $\pi$ -holes. As one specific example, tricoordinated triel atoms typically occur at the center of a planar triangle, with a  $\pi$ -hole located above the central triel atom [13,83–87], and the resulting triel bond [88–95] falls into the category of a  $\pi$ -hole bond. The  $\pi$ -hole situated above the C atom of a carbonyl group offers another common example, whose presence was manifested in early work of Burgi and Dunitz [96]. Protein structures can also involve participation of  $\pi$ -hole bonds [97,98], as is also true of self-assembling systems [99]. As work has progressed, there has been recognition of  $\pi$ -holes as providing a means by which an aerogen bond (involving rare gas atoms) can form [100–104]. Other newly introduced types of  $\sigma/\pi$ -hole directed interactions are alkali and alkaline earth bond (e.g., beryllium bond, magnesium bond) in which atoms of 1st and 2nd groups contribute [105–109] or regium and spodium bonds which employ transition metals from 11th (regium [110–115]) or 12th (spodium [105,116–119]) groups of the periodic table. The full range of these sorts of bonds, along with their designations, is summarized in Figure 1.

Alkali bond		Alkaline earth bond		Regium bond		Spodium bond		Triel bond		Tetrel bond		Pnicogen bond		Chalcogen bond		Halogen bond		Aerogen bond	
H	He	Li	Be	B	C	N	O	F	Ne	Na	Mg	Al	Si	P	S	Cl	Ar	K	Kr
Na	Mg	K	Ca	Sc	Ti	V	Cr	Mn	Fe	Co	Ni	Cu	Zn	Ga	Ge	As	Se	Br	Kr
Rb	Sr	Y	Zr	Nb	Mo	Tc	Ru	Rh	Pd	Ag	Cd	In	Sn	Sb	Te	I	Xe	Cs	Ba
Cs	Ba	Hf	Ta	W	Re	Os	Ir	Pt	Au	Hg	Tl	Pb	Bi	Po	At	Rn	Fr	Ra	
Rf	Db	Sg	Bh	Hs	Mt	Ds	Rg	Cn	Nh	Fl	Mc	Lv	Ts	Og					
La	Ce	Pr	Nd	Pm	Sm	Eu	Gd	Tb	Dy	Ho	Er	Tm	Yb	Lu					
Ac	Th	Pa	U	Np	Pu	Am	Cm	Bk	Cf	Es	Fm	Md	No	Lr					

Figure 1. Family of  $\sigma$  and  $\pi$ -hole interactions.

There have been a number of earlier reviews addressing the issue of  $\sigma$ -hole and  $\pi$ -hole bonds [13,49,51,52,81,84,105,120,121]. However, little attention has been devoted to situations where both hole types are present on a single molecule, and the competition between the two for a nucleophile. Indeed, it is also of intense interest to examine the result when both of these bonds are present at the same time. As has already been explored, the tunability of single  $\sigma$  or  $\pi$ -holes enables the construction of interesting assemblies with desired properties [122–124]. The possibilities multiply when both types of bonds are present and influence one another.

The driving goal for this work is to review with a critical eye what is known about systems offering both  $\sigma$  and  $\pi$ -holes to an approaching nucleophile. Are there rules that can be used to predict which will be preferred? Is there a distinction depending on whether

both holes lie on the same atom or on different atoms of the same molecule? Different combinations are discussed where  $\pi$ -hole bonds of various types are combined with other noncovalent bonds, whether aerogen, halogen, tetrel, pnictogen, or chalcogen.

## 2. Origin of $\pi$ -Holes

The  $\sigma$ -hole has been well documented in the literature, along with its explanation as emanating from the pull of electron density along the axis of a covalent bond. The origin of a  $\pi$ -hole is similar in some ways, as it too relies on anisotropic distribution of charge. The fundamental origin and nature of a  $\pi$ -hole can be understood using  $\text{F}_2\text{GeO}$  as an example. This molecule is planar with  $C_{2v}$  symmetry. The NBO localized orbitals representing the  $\sigma$  and  $\pi$  bonding orbitals of the  $\text{Ge}=\text{O}$  bond exhibited in the top half of Figure 2 both show a bias toward the more electronegative O. The region above the Ge atom and on its right, toward the two F atoms, thus suffers from a depletion of electron density. This shift is reflected by the drop in the total electron density as the point of reference moves up and out of the molecular plane, culminating in the minimum of the black  $\rho$  curve in Figure 3 for  $\theta \sim 60^\circ$ . Such a density depletion above the molecular plane is commonly referred to as a  $\pi$ -hole, which is in turn responsible for a maximum of the red molecular electrostatic potential (MEP) curve in Figure 3, which occurs at roughly  $\theta = 75^\circ$ . Figure 4a illustrates this  $\pi$ -hole in the MEP as the blue region lying above (and below) the Ge and shifted slightly toward the two F atoms. It is thus natural for a nucleophile to then approach this  $\pi$ -hole from this direction, as exemplified by the complex with  $\text{NH}_3$  displayed in Figure 4b. It might be noted as well that the  $\pi^*$  orbital in Figure 2 is perfectly situated to act as electron acceptor from the lone pair of the  $\text{NH}_3$  nucleophile, another trademark of  $\pi$ -hole interactions. Note finally the geometrical distortion of the originally planar  $\text{F}_2\text{GeO}$  in Figure 4b as the O and F atoms are shifted away from the approaching nucleophile another common characteristic of  $\pi$ -hole bonds.

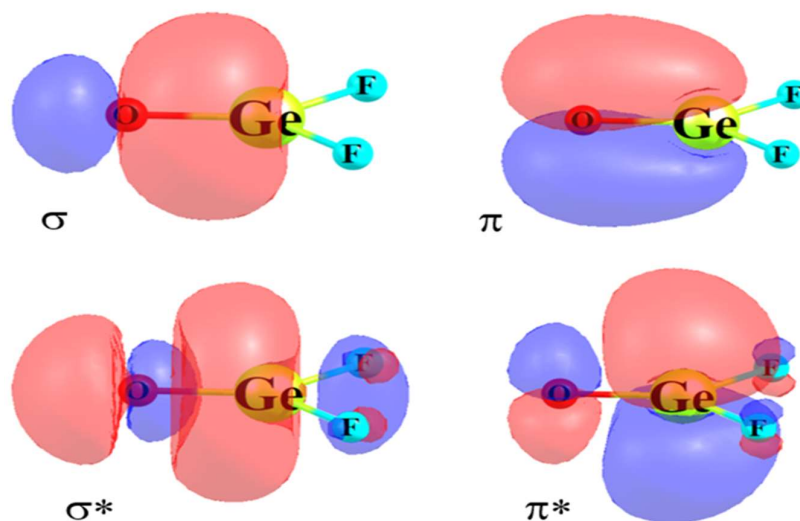


**Figure 2.** Ge-O NBO bonding and antibonding orbitals of  $\text{GeF}_2\text{O}$ . Red and blue colors indicate opposite phase of the wave function.

Of course, the forgoing explanation of the origin of a  $\pi$ -hole can vary from one system to the next. The presence of any lone electron pairs on the central atom can influence the magnitude and actual location of any such  $\pi$ -hole. An example to be discussed shortly is  $\text{XeF}_2\text{O}$  where the central Kr atom contains two such lone pairs. The positive region that appears above an aromatic ring of, e.g.,  $\text{C}_6\text{F}_6$ , is not located directly above any one C atom but lies rather above the ring's center. Such a dislocation can at times make it problematic to connect a  $\pi$ -hole with any particular atom, such as that above a  $\text{C}\equiv\text{N}$  group which lies roughly midway between the C and N atom.

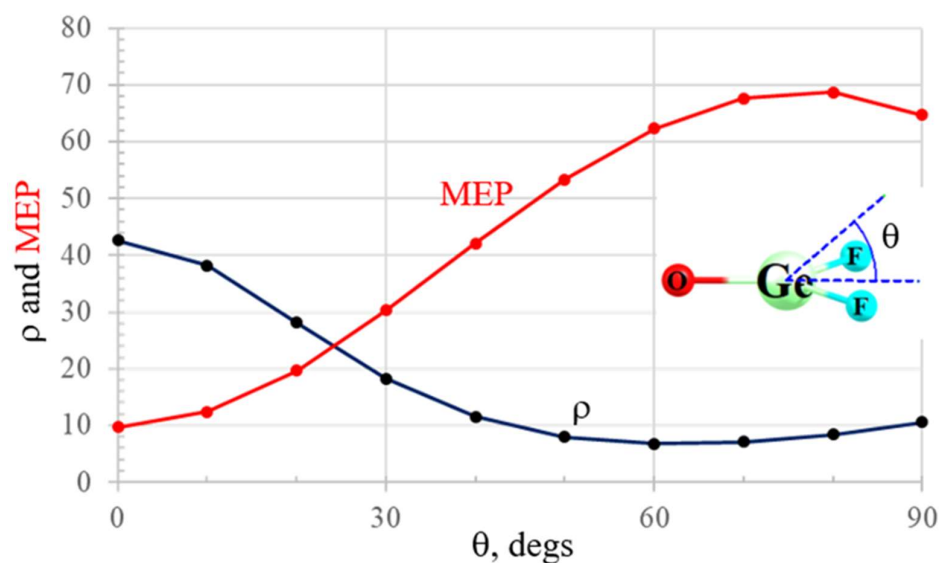


**Figure 3.** Electron density ( $10^{-5}$  au) and molecular electrostatic potential (MEP) ( $10^{-3}$  au) of  $\text{GeF}_2\text{O}$  as a function of the displacement from the molecular plane  $\theta$ , at a distance of  $2.5 \text{ \AA}$  from the Ge atom.

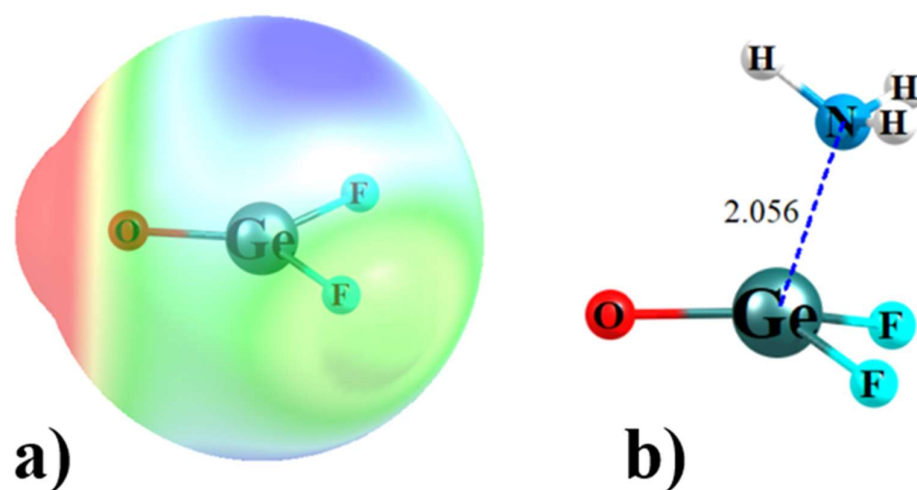


**Figure 4.** (a) MEP on surface of  $\text{GeF}_2\text{O}$  defined as  $1.5 \times \text{vdW}$  atomic radii. Blue and red colors refer to  $+0.05$  and  $-0.05$  au, respectively. (b) Optimized complex of  $\text{GeF}_2\text{O}$  with  $\text{NH}_3$  at the  $\text{mp2/aug-cc-pVDZ}$  level, with distance in  $\text{Å}$ .

It should be reiterated that the causality is as follows: depletion of electron density causes a rise in the electrostatic potential [125]. In fact, sometimes a hole is labeled as such even though the potential is not positive, just less negative than its surroundings. For practical reasons, the magnitude of a hole is typically measured on the  $0.001$  au electron isodensity surface and is quantified by the  $V_{S,\text{max}}$  parameter developed for this purpose [12,126]. The electron density can be accessed not only by quantum calculations but also experimentally by diffraction methods [127].

It has been shown that the intensity of a  $\sigma$ -hole can be adjusted by changing the polarizability of the central atom and the electron-withdrawing power of its substituents [13,84,127], and the same considerations apply to  $\pi$ -holes as well [128]. However, it must be borne in mind that the strength of a given interaction is not a function solely of electrostatic considerations. Polarization and dispersion forces are important attractive forces as well [13,17,129–131].

### 3. $\sigma$ -Hole and $\pi$ -Hole on the Same Atom

There are only a few reports in the literature of systems where both  $\sigma$  and  $\pi$  holes appear on the same atom. One example of such a situation is furnished by  $AeF_2O$  where  $Ae$  refers to an aerogen atom Kr or Xe [132]. As may be seen in Figure 5, the  $Ae$  atom of this molecule contains a  $\sigma$ -hole along the  $O=Ae$  bond extension, while a  $\pi$ -hole opens up above the molecular plane. As may be seen in the upper section of Table 1, the  $\sigma$ -hole is quite a bit more intense than the  $\pi$ -hole. The weaker nature of the latter may be attributed in part to the presence of lone pairs on the central  $Ae$  atom which share space with these holes and would dilute any density depletion. It is interesting to note that whereas the  $\sigma$ -hole is a bit more intense for Xe vs Kr, the reverse order is seen in their  $\pi$ -holes.

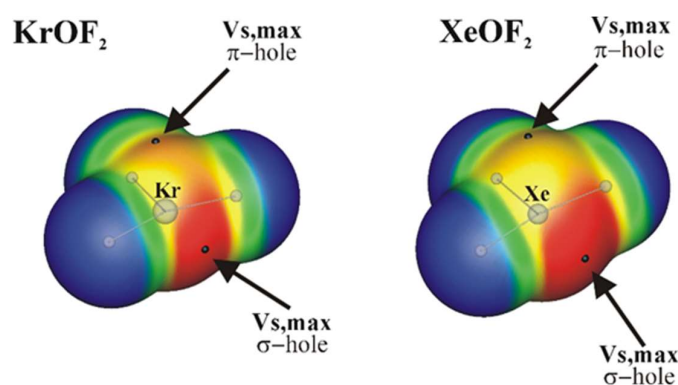


**Figure 5.** MEP of the isolated  $KrOF_2$  and  $XeOF_2$  molecules on the 0.001 au contour of the electron isodensity, at the MP2/aug-cc-pVDZ level. Color ranges, in kcal/mol, are red, greater than 40, yellow; between 20 and 40, green; between 0 and 20, blue, less than 0 (negative). Selected surface critical points  $V_{s,max}$  ( $\sigma$  and  $\pi$ -holes) are indicated as black dots. Reproduced from Reference [132] with permission from the PCCP Owner Societies.

These two  $AeF_2O$  molecules were allowed to react with a series of diazine nucleophiles (with negative MEP minima on the N atoms) [132]. It was found that the intensity of these various holes carries over into the interaction energies ( $E_{int}$ ) of the corresponding dimers. Complexation through the  $\sigma$ -hole was more stable than the corresponding  $\pi$ -hole dimers by about 6 kcal/mol. The stability order was parallel to the hole intensities, as the Xe complexes were slightly stronger than Kr atom analogues.

Another study by Bauza and Frontera [104] of related complexes obtained a deeper  $\sigma$ -hole on  $XeOF_2$  by a different computational procedure.  $XeOF_2$  complexes with ammonia and  $CH_3CN$  were characterized by similar interaction energies as in Reference [132]. Interaction energies were magnified by the use of an anion as nucleophile as would be expected. Unfortunately, these authors did not consider  $\pi$ -hole complexes for purposes of comparison.

**Table 1.** Comparison between  $\sigma$  and  $\pi$  hole depths in molecules where they coexist on the same atom,  $V_{S,max}$  in kcal/mol.

Molecule	Hole Source	Hole Type	$V_{S,max}$	References
Aerogen Bond Donors				
KrOF <sub>2</sub>	Kr	$\sigma$	58.7	[132]
KrOF <sub>2</sub>	Kr	$\pi$	39.1	[132]
XeOF <sub>2</sub>	Xe	$\sigma$	63.4	[132]
XeOF <sub>2</sub>	Xe	$\sigma$	90	[104]
XeOF <sub>2</sub>	Xe	$\pi$	36.2	[132]
Pnicogen Bond Donors				
PF <sub>2</sub> C <sub>6</sub> H <sub>5</sub>	P	$\sigma$	19.4	[133]
PF <sub>2</sub> C <sub>6</sub> H <sub>5</sub>	P	$\pi$	36.2	*
AsF <sub>2</sub> C <sub>6</sub> H <sub>5</sub>	As	$\sigma$	28.2	[133]
AsF <sub>2</sub> C <sub>6</sub> H <sub>5</sub>	As	$\pi$	44.0	*
SbF <sub>2</sub> C <sub>6</sub> H <sub>5</sub>	Sb	$\sigma$	38.4	[133]
SbF <sub>2</sub> C <sub>6</sub> H <sub>5</sub>	Sb	$\pi$	56.6	*
BiF <sub>2</sub> C <sub>6</sub> H <sub>5</sub>	Bi	$\sigma$	52.6	[133]
BiF <sub>2</sub> C <sub>6</sub> H <sub>5</sub>	Bi	$\pi$	60.9	*
PF <sub>3</sub>	P	$\sigma$	35.6	[134]
PF <sub>3</sub>	P	$\pi$	9.7	[134]
AsF <sub>3</sub>	As	$\sigma$	43.9	[134]
AsF <sub>3</sub>	As	$\pi$	7.1	[134]
SbF <sub>3</sub>	Sb	$\sigma$	51.6	[134]
SbF <sub>3</sub>	Sb	$\pi$	10.6	[134]
BiF <sub>3</sub>	Bi	$\sigma$	61.5	[134]
BiF <sub>3</sub>	Bi	$\pi$	12.7	[134]
Chalcogen Bond Donors				
SF <sub>4</sub>	S	$\sigma$	41.7	[135]
SF <sub>4</sub>	S	$\pi$	64.4	[135]**
SeF <sub>4</sub>	Se	$\sigma$	51.2	[135]
SeF <sub>4</sub>	Se	$\pi$	61.1	[135]**
TeF <sub>4</sub>	Te	$\sigma$	59.2	[135]
TeF <sub>4</sub>	Te	$\pi$	54.5	[135]**
PoF <sub>4</sub>	Po	$\sigma$	76.3	[135]
PoF <sub>4</sub>	Po	$\pi$	53.2	[135]**
Tetrel Bond Donors				
SiF <sub>4</sub>	Si	$\sigma$	127.3	[136]
SiF <sub>4</sub>	Si	$\pi$	109.8	[136]
GeF <sub>4</sub>	Ge	$\sigma$	120.9	[136]
GeF <sub>4</sub>	Ge	$\pi$	106.1	[136]
SnF <sub>4</sub>	Sn	$\sigma$	129.4	[136]
SnF <sub>4</sub>	Sn	$\pi$	121.3	[136]
PbF <sub>4</sub>	Pb	$\sigma$	127.3	[136]
PbF <sub>4</sub>	Pb	$\pi$	104.1	[136]

\* Value obtained by additional calculations for the purpose of the current review, at the same level as in Reference [136]. \*\* Values obtained for monomer in deformed complex geometry.

The ability of XeOF<sub>2</sub> to interact with a Lewis base through both hole types was considered [137] in connection with the nucleophile NCCH<sub>3</sub>, as displayed in Figure 6. The  $\sigma$ -hole complex on the left has the a shorter Xe $\cdots$ N distance than the  $\pi$ -hole structure by

nearly 0.4 Å, and is preferred by 2–4 kcal/mol. This energetic advantage occurs despite the presence of a secondary C...O tetrel bond in the latter. The authors questioned the level of covalency in the Xe...N bond, but their topological analyses were not conclusive. Unfortunately, this work did not delve into the  $\sigma$  or  $\pi$ -hole depths as background information.

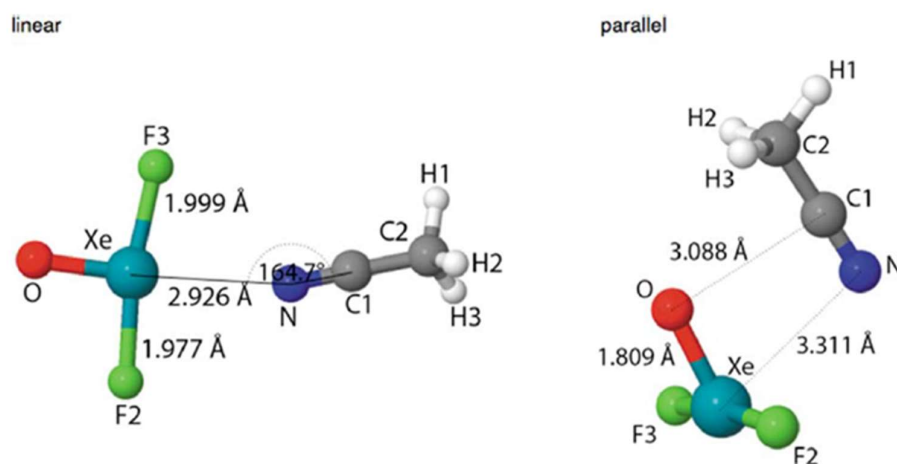


**Figure 6.** Two binding modes of  $\text{XeOF}_2 \cdots \text{NCCH}_3$  complexes, from Reference [137].

Brock et al. [138] provided experimental crystal structural evidence of the  $\text{XeOF}_2 \cdots \text{NCCH}_3$  binding wherein three different nucleophiles approached Xe from three different directions simultaneously, two of  $\pi$ -hole character and one  $\sigma$ -hole, demonstrating the viability of multiple bonds to different holes of the same atom. In a different vein, the  $\sigma$ -hole at Xe atom in  $\text{XeOF}_2$  has also been a vehicle by which to illustrate cooperativity between region and aerogen bond in the ternary systems of  $\text{C}_2\text{H}_2 \cdots \text{MCN} \cdots \text{XeOF}_2$ ,  $\text{C}_2\text{H}_4 \cdots \text{MCN} \cdots \text{XeOF}_2$ ,  $\text{MCN} \cdots \text{C}_2\text{H}_4 \cdots \text{XeOF}_2$  and  $\text{C}_2(\text{CN})_4 \cdots \text{MCN} \cdots \text{XeOF}_2$  where M = Cu, Ag or Au [111]. The  $\sigma$ -hole was able to interact with a N lone pair as well as the unsaturated  $\pi$ -system of a C=C bond. It would have been particularly interesting had the authors considered similar questions with regard to the Xe  $\pi$ -hole.

Within a hypervalent bonding situation, halogen atoms are also capable of containing a  $\pi$ -hole. Within the context of the  $\text{BrOF}_2^+$  cation [139] an X-ray structure indicated the central Br atom can be approached by three nucleophiles. Two  $\text{KrF}_2$  and one  $\text{AsF}_6$  molecule attack electrophilic regions on the outer surface of the Br atom. While these three Lewis bases appear to interact through  $\sigma$ -holes on the Br atom, it cannot be excluded that there is a  $\pi$ -hole site on this cation which can attract another Lewis base.

Turning to the pnicogen atom, interaction with  $\text{NH}_3$  [133] caused  $\text{ZF}_2\text{C}_6\text{H}_5$  (Z = P, As, Sb, Bi) to take on two different arrangements. The first contained three  $\sigma$ -holes in the range of 19–53 kcal/mol, the strongest for the most polarizable Bi atom. As indicated in Figure 7, approach to this  $\sigma$ -hole places the  $\text{NH}_3$  opposite one of the F atoms. Internal rearrangement of the  $\text{ZF}_2\text{C}_6\text{H}_5$  to a more planar structure opens up a  $\pi$ -hole above the Z atom. As delineated in Table 1, this hole has a magnitude between 36 and 61 kcal/mol, which can also attract the  $\text{NH}_3$  nucleophile, as depicted in the lower half of Figure 7. The greater depth of the  $\pi$ -holes leads to their larger interaction energies by a factor of 2 to 8. However, the internal rearrangement required to open up these  $\pi$ -holes is energetically costly, requiring between 16 and 43 kcal/mol, so that despite the greater depth of the  $\pi$  vs  $\sigma$ -holes, and their superior interaction energies, it is the set of structures in the top half of Figure 7 that are energetically preferred by a margin between 1 and 11 kcal/mol. This deformation energy diminishes with larger Z atoms, so that there is a closer competition between the  $\sigma$  and  $\pi$ -hole complex binding energies.

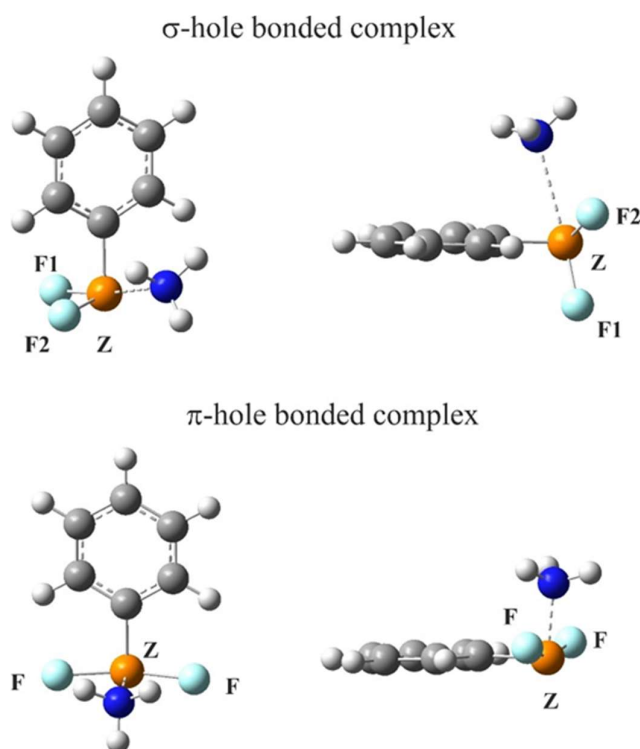


**Figure 7.** Two types of the MP2/aug-cc-pVDZ optimized structures (top and side views) of complexes of  $\text{NH}_3$  with  $\text{ZF}_2\text{C}_6\text{H}_5$ , from Reference [133].

Another study of pnictogen bonded systems addressed the question of how many Lewis base ligands can be attached to a single  $\text{ZF}_3$  molecule [134]. The  $\text{ZF}_3$  monomer ( $Z = \text{P}, \text{As}, \text{Sb}, \text{Bi}$ ) is characterized by three  $\sigma$ -holes, one opposite each  $\text{Z-F}$  bond, and a much shallower one that lies directly opposite the  $\text{Z}$  lone pair, amongst the three  $\text{F}$  atoms. Although  $\text{ZF}_3$  is pyramidal, the latter was considered a  $\pi$ -hole due to its placement. Table 1 documents the much lesser  $V_{\text{S,max}}$  of the latter as compared to the three  $\sigma$ -holes on each  $\text{ZF}_3$  unit. Because of its greater electrostatic attraction, it is the  $\sigma$ -hole that draws in the approaching nucleophile, whether  $\text{HCN}$ ,  $\text{CN}^-$ , or  $\text{NH}_3$ . A second nucleophile of any sort occupies a second  $\sigma$ -hole, but such a triad is only possible for the two heavier  $\text{Sb}$  and  $\text{Bi}$  atoms for the anionic  $\text{CN}^-$  due to the large Coulombic repulsion required to form such a dianion, and even so, the  $\text{SbF}_3 \cdots (\text{CN}^-)_2$  triad has a positive binding energy.  $\text{HCN}$  is too weak a nucleophile to squeeze in a third pnictogen-bonded base, while such a tetrad is possible for  $\text{NH}_3$ . Addition of a fourth  $\text{NH}_3$  is possible only for  $Z = \text{Bi}$ . It seems to occupy the  $\pi$ -hole mentioned above, but this weak interaction is reinforced by secondary noncovalent bonding, reflecting the reluctance of these units to engage with their weak  $\pi$ -holes.

Shifting attention to chalcogen bonding, the  $\text{YF}_4$  ( $Y = \text{S}, \text{Se}, \text{Te}, \text{Po}$ ) monomer adopts a see-saw equilibrium geometry [135] with a pair of  $\sigma$ -holes lying opposite each of the two equatorial  $\text{Y-F}$  bonds, with  $V_{\text{S,max}}$  magnitudes between 42 and 76 kcal/mol, as listed in Table 1. A pair of  $\text{NH}_3$  nucleophiles can approach along these two  $\sigma$ -holes which would lead to an overall octahedral arrangement with the two  $\text{NH}_3$  units *cis* to one another, as depicted on the left side of Figure 8. An alternative *trans* positioning of the two nucleophiles as shown on the right side of Figure 8 would place the central  $\text{YF}_4$  in a square pyramidal configuration, closer to a square. As such, it would acquire a  $\pi$ -hole directly below the  $\text{Y}$  atom. It may be observed from Table 1 that these  $\pi$ -holes are rather intense, between 53 and 64 kcal/mol, so can easily attract one of the two  $\text{NH}_3$  bases. The other side of the nearly square  $\text{YF}_4$  unit contains a  $\text{Y}$  lone electron pair, which obstructs the second  $\text{NH}_3$  from approaching directly opposite the first, so it situates itself closer to a point opposite one of the  $\text{Y-F}$  bonds, close to its  $\sigma$ -hole. The energetic comparison of the *cis* and *trans*

geometries must again consider both interaction and deformation energies. Whereas the interaction energies of the *trans* structure are much more negative than those for *cis*, the deformation energies required to adopt the nearly square structure are much larger as well. The net result is that the binding energies of the *cis* and *trans* conformations are comparable to one another. *Cis* is favored for the two smaller S and Se chalcogen atoms, while the heavier Te and Po, with their somewhat reduced deformation energy requirements, shift the equilibrium toward *trans*.

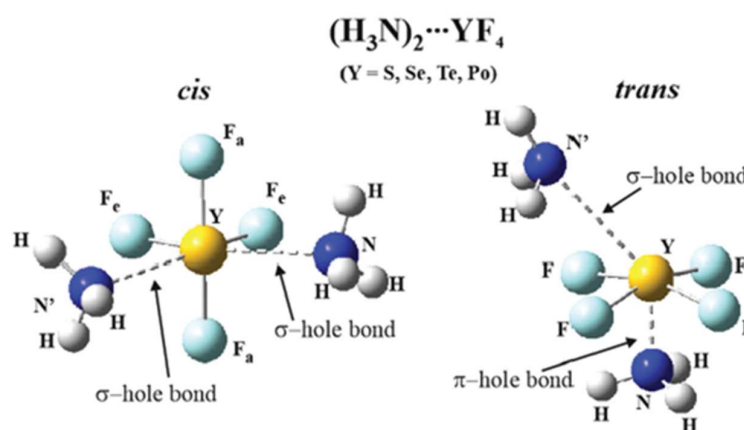


**Figure 8.** Cis and Trans arrangements of two  $\text{NH}_3$  units complexed with  $\text{YF}_4$  via chalcogen bonds. Reproduced from Reference [135] with permission from the PCCP Owner Societies.

Similar considerations apply to tetrel bonds.  $\text{TF}_4$  ( $\text{T} = \text{Si}, \text{Ge}, \text{Sn}, \text{Pb}$ ) is of course tetrahedral, so is characterized by four equivalent  $\sigma$ -holes opposite each T-F bond [136]. In order to accommodate a pair of bases,  $\text{TF}_4$  distorts into an octahedron. *Cis* approach of the two bases places the  $\text{TF}_4$  in a see-saw geometry with a pair of  $\sigma$ -holes, each lying opposite an equatorial T-F. An alternate deformation into a square planar structure, allowing for *trans* arrangement of the two bases, imparts a pair of  $\pi$ -holes to the  $\text{TF}_4$  unit. The lowermost section of Table 1 shows the  $\sigma$ -holes of the former structure are slightly deeper than the  $\pi$ -holes of the latter. It is worth stressing that either type of hole in these distorted arrangements, whether see-saw or square, is considerably deeper than those in the original undistorted tetrahedral geometry. The interaction energies of the pair of NCH bases with the square was considerably more negative than for the see-saw, despite the larger  $V_{S,\text{max}}$  for the latter, by between 10 and 40 kcal/mol. On the other hand, the energy required to deform the tetrahedral  $\text{TF}_4$  into a square far exceeded that needed for the see-saw, particularly for the smaller T atoms. In quantitative terms, the deformation energies for the squares varied from 22 all the way up to 66 kcal/mol for  $\text{SiF}_4$ , as compared to only 0.4–15 kcal/mol for the see-saw. The net result is that it is the *cis* geometry that is favored, and this preference varies from only 3 kcal/mol for  $\text{PbF}_4$  up to 23 kcal/mol for  $\text{SiF}_4$ . In fact, the large deformation energies for the square structures with small T make the binding energy a positive quantity for both  $\text{SiF}_4$  and  $\text{GeF}_4$ .

The forgoing highlights the importance of considering  $\pi$ -holes, even for Lewis acids whose undistorted monomer geometries are such that no such holes are present. The deformations which the monomer undergoes in its interaction with one or more bases can present the possibility of a  $\pi$ -hole whose interaction is comparable to, or even stronger than, that with the original  $\sigma$ -holes.

#### 4. $\sigma$ -Hole and $\pi$ -Hole on Different Atoms

More common than the presence of a  $\sigma$  and  $\pi$ -hole arising on the same atom is the situation wherein these two holes are located on different atoms. Within this subgroup there are several themes that are more common than others.

#### 4.1. Combination of $\sigma$ -Hole on Halogen or Chalcogen with $\pi$ -hole on Aromatic Ring

A number of works have considered situations wherein a  $\sigma$ -hole on a halogen (X) atom coexists with a  $\pi$ -hole lying above the plane of an aromatic ring. When not directly above the center of the ring, the  $\pi$ -hole is shifted so as to lie closer to the midpoint of a C-C or C-N bond, a topic which has been discussed at some length elsewhere [140]. With this understanding, this review subsumes all of these types into the category of  $\pi$ -hole. Values of the MEP positive maxima are enumerated in Table 2.

One prominent example modeled functionalization of graphene sheets by  $C_6H_5Br$  [141] and its physisorption on the graphene surface through either its Br  $\sigma$ -hole or phenyl  $\pi$ -hole. The adsorption energy with electron-rich graphene regions was three times larger for the  $\pi$ -hole interaction than for the  $\sigma$ -hole contact. Taking the analysis one step further, the authors noted that the adsorption seriously affects the properties of graphene. Bromopentafluorobenzene also has the option of interaction through either its  $\sigma$  or  $\pi$ -hole [142], in this case with pyridine. The latter nucleophile was able to interact either through its N lone pair or the  $\pi$ -electron system of its aromatic ring. As in the previous case the  $\pi$ -hole $\cdots\pi$  interaction yielded the more stable dimer, here by about 4 kcal/mol. As a fundamental point of distinction, energy decomposition suggested that whereas electrostatics is the dominant factor in  $\sigma$ -hole complexation, this role is assumed by dispersion in  $\pi$ -hole bonding. Another study of this type [143] involved homo-dimerization of 1,3,5-trifluoro-2,4,6-triiodobenzene (TITFB) through its  $\sigma$  or  $\pi$  holes. The  $\sigma$ -hole on the iodine atom was roughly three times deeper than the  $\pi$ -hole positioned above the benzene ring. However, the intermolecular distance was shorter of about 0.1 Å in the case of  $\pi$ -hole interaction.

**Table 2.** Comparison between  $\sigma$  and  $\pi$  holes appearing on the same molecule, where  $\sigma$ -hole is coupled with halogen (or chalcogen) atom and  $\pi$ -hole with an aromatic ring,  $V_{S,max}$  in kcal/mol.

Molecule	Hole Source	Hole Type	$V_{S,max}$	References
1,4-DITFB	I	$\sigma$	32.3	[140]
	Carbon/Benzene ring	$\pi$	15.1	[140]
$C_6H_5Br$	Br	$\sigma$	up to ~15	[142]
	Benzene Ring	$\pi$	up to ~15	[142]
TITFB	I	$\sigma$	30.1	[143]
	Carbon/Benzene Ring	$\pi$	11.4	[143]
Halogen Substituted 1,3,4-oxadiazol-2(I)3(H)-thiones	S (Chalcogen), Cl, Br	$\sigma$	up to ~37	[144]
	Oxadiazole and Benzyl Ring	$\pi$	up to ~37	[144]
Haloperfluorobenzene	Cl, Br, I	$\sigma$	20.9 to 32.8	[145]
	Benzene Ring	$\pi$	12.6 to 19.8	[145]
$XC_3H_4N_2^+$ ; X = F, Cl, Br, I	Cl, Br, I	$\sigma$	105.9 to 117.5	[146]
	Imidazolium Ring	$\pi$	111.0 to 127.9	[146]

Shukla et al. [144] found that biologically active derivatives of halogen substituted 1,3,4-oxadiazol-2(I)3(H)-thiones in the solid state contain a  $\sigma$ -hole on the S, Cl, and Br atoms and a  $\pi$ -hole above the oxadiazole and benzyl rings all of which participate in noncovalent interactions. The S $\cdots$ N  $\sigma$ -hole chalcogen bond manifested distinctive activity in stabilization of these amalgams. This work fits into the idea that both  $\sigma$  and  $\pi$ -hole bonding play a pivotal role in the 3D organization of crystalline structures and in various molecular scaffolds.

Li et al. provided another example [145] in the context of interactions between haloperfluorobenzene with fluoroanthene (FA) which assemble into nine luminescent cocrystals. These interactions involved the participation of the  $\sigma$ -hole of Cl, Br, or I atoms or the

$\pi$ -hole of the phenyl ring with aromatic  $\pi$ -electrons on the FA. The  $\sigma$ -holes were more intense than the  $\pi$ -hole by as much as 17 kcal/mol. While the balance between  $\sigma$  and  $\pi$ -hole bonding with FA varied as the  $\sigma$ -hole deepened and the  $\pi$ -hole weakened along with the growth of the halogen atom, it was nonetheless the  $\sigma$ -hole $\cdots\pi$  interaction that was universally favored.

Wang et al. [146] examined the interaction between protonated 2-halogenated imidazolium cation ( $\text{XC}_3\text{H}_4\text{N}_2^+$ ; X = F, Cl, Br, I) and the set of  $(\text{CH}_3)_3\text{SiY}$  (Y = F, Cl, Br, I) Lewis bases. The acid contained both a  $\sigma$ -hole on its X atom and a  $\pi$ -hole above the imidazolium ring. The  $\pi$ -holes were the deeper of the two, leading to stronger interactions. In these ionic cases, both interaction types were driven mainly by electrostatic forces (the electrostatic term was well correlated with the  $V_{S,\text{max}}$  values found on monomers) with some addition of polarization and dispersion. The dispersion term was somewhat more prominent for the weaker  $\sigma$ -hole complexes while the polarization component towered over dispersion for  $\pi$ -hole dimers.

An experimental component was contributed by Zhang et al. [147], which paired  $\text{C}_6\text{F}_5\text{X}$  (X = Cl, Br, I) with  $\text{C}_6\text{D}_6$  in solution. As in the earlier cases, a  $\sigma$ -hole appeared on the X atom while a  $\pi$ -hole occupied the space above the aromatic ring. For the strongest  $\sigma$ -hole which was associated with the I atom, the interaction lay through its  $\sigma$ -hole, while it was the  $\pi$ -hole link that dominated for the smaller halogens. This pattern was attributed by the authors in large part to entropic contribution since enthalpy alone would not be sufficient to stabilize  $\sigma$ - $\pi$  over  $\pi$ - $\pi$ . Comparable conclusions were drawn in another paper by the same group [148], where Lewis acids participated in complexes with deuterated solvent molecules with lone-pair electrons, including  $\text{CD}_3\text{CN}$ ,  $\text{CD}_3\text{COCD}_3$ ,  $\text{CD}_3\text{OD}$ , and  $[\text{D}_6]\text{DMSO}$ . Experiment and calculations showed that again  $\sigma$ -hole and  $\pi$ -hole bonds compete with each other for the nucleophile's lone pair, rather than the  $\pi$ -electron system of  $\text{C}_6\text{D}_6$  in the earlier work. The results indicated that only the iodine and a few bromine  $\sigma$ -hole halogen bonds are strong enough to contend successfully with the  $\pi$ -hole interactions in solution.

The biologically relevant ebselen derivative, 2-(2-bromophenyl)benzo[d][1,2]selenazol-3(2H)-one homodimer [149] exhibited markers of simultaneous  $\sigma$ -hole and  $\pi$ -hole bonding. The  $\sigma$ -hole lay along the C-Br covalent bond elongation and the  $\pi$ -hole was derived from the phenyl ring. Shukla et al. postulated two simultaneous interactions:  $\sigma$ -hole bonding from the Br  $\sigma$ -hole to the negative charge-concentrated C-C bond, as well as a  $\pi$ -hole bond between a positively charged C atom and the lone electron pair of Br, confirmed by their NBO analysis. This case represents an uncommon model wherein the same atom acts as both  $\sigma$ -hole bond acceptor and  $\pi$ -hole bond donor.

Finally, Wang et al. [140] reviewed a comparison between complexes stabilized by  $\sigma/\pi$  holes with various nucleophilic acceptors with particular emphasis on their potential application to anion recognition and transport. Among numerous examples, one of especial interest concerned 1,4-diiodoperfluorobenzene (1,4-DITFB) with both a  $\sigma$  and  $\pi$ -hole. The former was twice as deep as the latter, and the authors underscored that this molecule can act as  $\sigma/\pi$  hole donor and also by taking into account the high amount of electronic density collected on F atoms, and on the belt around the central fragments of the I atoms surface, it can serve as  $\sigma$ -hole or  $\pi$ -hole acceptor as well.

#### 4.2. Combination of $\sigma$ -Hole Halogen Bond with Other $\pi$ -Hole Sources

Further exploration of the literature supplies examples where a X  $\sigma$ -hole is combined with  $\pi$ -holes derived from groups other than aromatic rings. Instances of the halogen-pnictogen combination are most numerous. Lang et al. [150] provided a textbook example in that the surface of  $\text{XONO}/\text{XONO}_2$  (X = F, Cl, Br, I) contains both a typical  $\sigma$ -hole on X and a  $\pi$ -hole localized on the N atom. The  $V_{S,\text{max}}$  values for this set of systems are listed in the first four rows of Table 3. The authors observed that the  $\sigma$ -hole intensity grew in line with the increase of X atom size whereas the  $\pi$ -hole magnitude dropped in this same order (similar picture as at Li et al. [145]). Binary complexes of these monomers

with ClO and ammonia had interaction energies correlated to the MEP maxima. The ternary ClO...XONO/XONO<sub>2</sub>...NH<sub>3</sub> complexes revealed anti-cooperative effect between the  $\sigma$ -hole halogen and  $\pi$ -hole pnictogen bond, as expected when the central unit acts as double electron acceptor. Solimannejad et al. [151] examined adducts of NO<sub>2</sub>X (X = Cl, Br) with HCN and HNC moieties. The  $\pi$ -hole was stronger than the  $\sigma$ -hole, contrary to the Lang et al. results. Within four tested interaction schemes in binary complexes (stabilized by  $\sigma$ -hole,  $\pi$ -hole and two different hydrogen bond approaches), those bonded through the  $\pi$ -hole were the most stable, for the majority of the trimers displayed negative cooperativity between the  $\sigma$  and  $\pi$ -hole interactions. Subsequent work of this research group [152] deployed the NO<sub>2</sub>I monomer with a different Lewis base (ammonia). The I atom showed a deeper  $\sigma$  than  $\pi$ -hole, which led to the expected outcome that the NO<sub>2</sub>I dimer with ammonia was more strongly bound by its  $\sigma$  than by its  $\pi$ -hole. This study also supported two conclusions formulated in earlier cited works: (i) both interaction types showed a strong correlation between  $V_{S,max}$  and interaction energy, and (ii) antagonistic effect between  $\sigma$  and  $\pi$ -hole bonds was observed in trimers with two ammonia units.

**Table 3.** Comparison between  $\sigma$  and  $\pi$  holes appearing on the same molecule, where  $\sigma$ -hole is coupled with halogen atom and  $\pi$ -hole with different sources (other than aromatic ring),  $V_{S,max}$  in kcal/mol.

Molecule	Hole Source	Hole Type	$V_{S,max}$	References
Halogen-Pnictogen				
XONO (X = F, Cl, Br, I)	X	$\sigma$	−6.3 to 51.1	[150]
XONO (X = F, Cl, Br, I)	N	$\pi$	20.8 to 29.5	[150]
XONO <sub>2</sub> (X = F, Cl, Br, I)	X	$\sigma$	2.7 to 67.7	[150]
XONO <sub>2</sub> (X = F, Cl, Br, I)	N	$\pi$	29.6 to 41.2	[150]
NO <sub>2</sub> X (X = Cl, Br)	X	$\sigma$	13.2 and 19.0	[151,152]
NO <sub>2</sub> X (X = Cl, Br)	N	$\pi$	28.1 and 29.8	[151,152]
NO <sub>2</sub> I	I	$\sigma$	29.4	[152]
NO <sub>2</sub> I	N	$\pi$	23.5	[152]
Halogen-Tetrel				
NCX (X = F, Cl, Br)	X	$\sigma$	14.3 to 42.1	[153]
NCX (X = F, Cl, Br)	C	$\pi$	12.4 to 27.3	[153]
Halogen-Trirel				
BH <sub>2</sub> X (X = F, Cl, Br, I)	Cl, Br, I	$\sigma$	3.5 to 11.3	[154]
BH <sub>2</sub> X (X = F, Cl, Br, I)	B	$\pi$	28.8 to 39.4	[154]
Halogen-Beryllium				
BeCl <sub>2</sub>	Cl	$\sigma$	1.2	[109]
BeCl <sub>2</sub>	Be	$\pi$	32.2	[109]

There are also examples in the literature combining a  $\sigma$ -halogen with a  $\pi$ -tetrel bond. As one example, McDowell [153], analyzed complexes of NCX (X = F, Cl, Br) with H<sub>2</sub>O. Besides the obvious appearance of a  $\sigma$ -hole on X, a  $\pi$ -hole region was noticed above and below C. As in the previous cases, the intensity of the  $\pi$ -hole drops along with larger X as its  $\sigma$ -hole deepens. Of the two potential binding modes illustrated in Figure 9, only NCF was able to form complexes with water via both modes a and b. Whereas the  $\pi$ -hole on NCF was 2.5 times stronger than its  $\sigma$ -hole, the  $\pi$ -holes on NCCl and NCBBr were too weak to attract the incoming nucleophile. With regard to addition of a third entity, addition of hydrogen and beryllium cations destabilized the  $\sigma$ -hole bond while improving binding in the  $\pi$ -hole complexes.

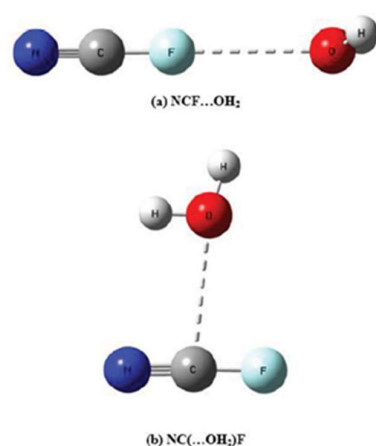


**Figure 9.** Optimized structures of NCF complexes with water stabilized by (a)  $\sigma$ -hole and (b)  $\pi$ -hole, from Reference [153].

Bauza and Frontera [154] tested the ability of  $\text{BH}_2\text{X}$  ( $\text{X} = \text{F}, \text{Cl}, \text{Br}, \text{I}$ ) to establish various sorts of interactions in their homodimers, depending on the attack angle between them. Along with the presence of a  $\sigma$ -hole on  $\text{X}$ , a  $\pi$ -hole was also available over the central  $\text{B}$ , perpendicular to the molecular plane. The strengths of these two holes followed expected trends based on  $\text{X}$  atomic size, and the  $\text{B}$   $\pi$ -hole was considerably more intense than the  $\text{X}$   $\sigma$ -hole. It was therefore no surprise to find a strong interaction energy of  $-34.7$  kcal/mol for  $\pi$ -hole( $\text{B}$ ) $\cdots\sigma$ -hole( $\text{I}$ ) interaction, much larger than that when  $\text{I}$  is replaced by  $\text{Br}$ , or even the halogen bond between  $\text{I}$   $\sigma$ -holes in a pair of  $\text{BH}_2\text{I}$  molecules.

A particularly unusual combination of holes was examined by Alikhani [109]. The  $\pi$ -hole on  $\text{BeCl}_2$  occurs as a narrow belt around the  $\text{Be}$  atom, with  $V_{\text{S,max}} = 32.2$  kcal/mol. The magnitude of the  $\sigma$ -hole on  $\text{Cl}$  is only 1.2 kcal/mol, too weak to expect effective attraction of a Lewis base. The author consequently focused on the nature and properties of the  $\pi$ -hole beryllium bond in complexes with nucleophiles  $\text{Cl}_2$ ,  $\text{NH}_3$ , and DMF (dimethylformamide), all of which proved to be quite strong, with the  $E_{\text{int}}$  reaching up to  $-46.3$  kcal/mol. One might expect that the replacement of the  $\text{Cl}$  on  $\text{BeCl}_2$  by  $\text{Br}$  or  $\text{I}$  would intensify the  $\text{X}$   $\sigma$ -hole and perhaps also weaken the  $\pi$ -hole on  $\text{Be}$ . If that were the case, then a  $\text{XB}$  through the  $\text{Br}$  or  $\text{I}$   $\sigma$ -hole might be able to successfully compete with the  $\text{Be}$   $\pi$ -hole interaction.

#### 4.3. Other Examples

The literature contains a few other sorts of combinations of  $\sigma$  with  $\pi$ -holes. Pal et al. [155] present the interplay between these binding sites in Fmoc-Leu- $\Psi$ [ $\text{CH}_2\text{NCS}$ ] (Fmoc = fluorenylmethyloxycarbonyl protecting group, Leu = leucine) organic isothiocyanate which act as an intermediate in the synthesis of bioactive peptides. The  $\text{N}=\text{C}=\text{S}$  group contains a  $\sigma$ -hole on the  $\text{S}$  atom surface (along the extension of the  $\text{C}=\text{S}$  bond), and a  $\pi$ -hole perpendicular to the  $\text{C}-\text{N}$  bond. The specific location of the  $\pi$ -hole makes it difficult to classify as either a  $\pi$ -hole tetrel or pnictogen bond. For the purpose of the current review, it was classified as  $\pi$ -hole tetrel/pnictogen bond (see Table 4). Between these positively charged sections, there were also regions of negative potential derived from the lone electron pair of the nitrogen ( $\sigma$ -hole acceptor) and sulphur ( $\pi$ -hole acceptor) atoms.  $\text{N}=\text{C}=\text{S}\cdots\text{N}=\text{C}=\text{S}$  contacts were observed in the crystal lattice that are associated with electrostatically driven attractions between regions of opposite charge. These simultaneous  $\sigma$  and  $\pi$ -holes interactions with the negative sites were cooperative, thereby magnifying the stabilization within the crystal.

The specific location of the  $\pi$ -hole was more definitive [156] in  $\text{CF}_2=\text{CFZH}_2$  ( $\text{Z} = \text{P}, \text{As}, \text{Sb}$ ) and  $\text{CF}_2=\text{CFPF}_2$ . The electron-deficient regions corresponding to  $\pi$ -holes were positioned directly above the  $\text{C}$  atom, while the  $\sigma$ -hole was localized on the pnictogen  $\text{Z}$  atom. The  $\sigma$ -hole became deeper in the sequence  $\text{P} < \text{As} < \text{Sb}$  attributed to rising  $\text{Z}$  polarizability, while the  $\pi$ -hole magnitude lessens in the same order, as documented in

Table 4. Switching -PH<sub>2</sub> moiety to -PF<sub>2</sub> boosted the magnitude of both holes. The prediction of MEP extrema was verified by the energetic properties of the complexes formed between these Lewis acids and NH<sub>3</sub> or NMe<sub>3</sub>. The interaction energies of the dyads were generally consistent with the MEP trends. However, some irregularity was found, as the  $\sigma$ -hole complexes in each case were more stable than their  $\pi$ -hole counterparts, as might be expected for Z = As, Sb but counter to MEP trends for P. It is worth emphasizing, however, that the differences in energy between the two kinds of complexes were less than 0.5 kcal/mol. It might be concluded then that  $\sigma$ -hole and  $\pi$ -hole sites can compete with one another in these systems. Further analyses (NBO,  $E_{\text{int}}$  decomposition) revealed that the formation of the complexes is grounded not only in the electrostatic term (which nevertheless governs) but also charge transfer between subunits which varied from 0.3 up to 14.4 kcal/mol, for LP(N)  $\rightarrow$   $\sigma^*$ (C-Sb) donation. The scale of charge transfer was larger for  $\sigma$ -hole dimers than in the case of  $\pi$ -hole adducts.

**Table 4.** Comparison between other combinations of  $\sigma$  and  $\pi$  holes appearing on the same molecule,  $V_{S,\text{max}}$  in kcal/mol.

Molecule	Hole Source	Hole Type	$V_{S,\text{max}}$	References
Chalcogen-Tetrel/Pnicogen				
Fmoc-Leu- $\Psi$ [CH <sub>2</sub> NCS]	S	$\sigma$	3.9 (exp.), 7.8 (theory)	[155]
Fmoc-Leu- $\Psi$ [CH <sub>2</sub> NCS]	C=N bond	$\pi$	no data	[155]
Pnicogen-Tetrel				
CF <sub>2</sub> =CFZH <sub>2</sub> (Z = P, As, Sb)	Z	$\sigma$	19.4 to 28.9	[156]
CF <sub>2</sub> =CFPF <sub>2</sub>	C	$\pi$	36.4	[156]
CF <sub>2</sub> =CFZH <sub>2</sub> (Z = P, As, Sb)	Z	$\sigma$	25.7 to 28.2	[156]
CF <sub>2</sub> =CFPF <sub>2</sub>	C	$\pi$	40.1	[156]
Tetrel-Tetrel				
F <sub>2</sub> C=CFTF <sub>3</sub> (T = C, Si, Ge)	T	$\sigma$	8.2 to 46.4 *	[157]
F <sub>2</sub> C=CFTF <sub>3</sub> (T = C, Si, Ge)	C=C Bond	$\pi$	30.7 to 35.1 *	[157]

\* In cited work, these values are probably given in wrong unit (eV instead of more reliable au).

Another work by this group [157] involved the F<sub>2</sub>C=CFTF<sub>3</sub> (T = C, Si, and Ge) as Lewis acid with water, ammonia, or formaldehyde as Lewis base, comparing the  $\sigma$  or  $\pi$ -holes on the tetrel T atoms. The  $\sigma$ -hole was formed along the T-F bond while the  $\pi$ -hole appeared perpendicular to the C=C double bond, coplanar to the  $\sigma$ -hole. The  $\pi$ -hole maxima rose along with the T atom size, in contrast to the case in earlier studies. However, the magnitudes were quite limited and for T = C and Si, the  $\pi$ -hole intensities were very close to one another. One can assume that the  $\pi$ -hole connected with the C=C bond is much less sensitive to the remainder of the molecule. The MEPs of the  $\sigma$ -holes were mostly consistent with previous patterns and also increased with the enlargement of T. The  $\pi$ -hole was stronger than the  $\sigma$ -hole in F<sub>2</sub>C=CFCF<sub>3</sub> while the reverse was observed for T = Si and Ge. In keeping with this MEP data, F<sub>2</sub>C=CFCF<sub>3</sub> prefers to form a  $\pi$ -hole tetrel bond whereas F<sub>2</sub>C=CFSiF<sub>3</sub> and F<sub>2</sub>C=CFGeF<sub>3</sub> were prone to a  $\sigma$ -hole tetrel bond. The strong correlation between MEP and interaction energy of the dimers was confirmed.

## 5. Conclusions and Prospective

Molecular systems can contain both  $\sigma$ - and  $\pi$ -holes, and there is a growing literature on both of them that allow some comparisons to be drawn. The presence of both sorts of holes is reflected in an expansion of possible binding sites and an increased flexibility in the noncovalent bonding with nucleophiles. The examination of crystals displays this flexibility in an array of binding patterns [104,140–146,149,153,155] where the directionality of  $\sigma/\pi$ -hole bonds is integral to arrangement, stabilization, and self-organization. There

are numerous examples where these interactions are important to systems with biological connections [144,149,155] or photophysical performance [141,143,145].

In addition to the crystallographic data and their supporting theoretical investigations, examinations of systems in solution or model geometries in the gas phase provide additional insights into mutual presence of both  $\sigma$  and  $\pi$ -holes. The most-commonly observed situation to date is the combination of a  $\sigma$ -hole on a halogen atom with a  $\pi$ -hole from a variety of sources, most notably an aromatic ring. However, the full list is rather extensive, as for example when both sorts of hole occur on a single tetrel atom. One interesting conclusion is that a particular sort of hole does not have to be present in the isolated monomer. For example, the approach of a nucleophile can induce geometric deformation into the Lewis acid which in turn causes the appearance of a  $\pi$ -hole that is not present in its isolated form.

Another pattern which has emerged from the studies is that a  $\sigma$ -hole typically deepens as the atom on which it occurs grows larger, e.g., Si < Ge < Sn, whereas this same enlarging atom can lead to a weakening of a  $\pi$ -hole. These opposing trends offer the opportunity to guide an emerging complex geometry based on atom size. When both hole types are present, they each offer an attractive site for binding by a nucleophile. However, since both bonding types utilize the Lewis acid as electron acceptor, the two bonds weaken one another in a negative cooperative manner.

Whether  $\sigma$  or  $\pi$ -hole type, the noncovalent bond appears to have a strong electrostatic component, based on rigorous calculations of this component, as well as a tight correlation of bond strength with the depth of the hole. However, these bonds rely to a large extent also on polarization and charge transfer effects, complemented by dispersive forces, although the precise mix of these different components varies from one bond to another. A slightly different perspective on some of these bonds has been offered by the Bickelhaupt group [22,23] in which emphasis is placed on the activation strain model of chemical reactivity and the energy decomposition analysis combined with molecular orbital theory.

It is hoped that this review of the current state of knowledge concerning these  $\sigma$  and  $\pi$ -hole bonds will motivate additional work to better refine our understanding of the forces that undergird and control them. In a practical sense, this enhanced knowledge base will hopefully lead to the development of new crystal packing motifs and to innovative materials with improved properties.

**Author Contributions:** Conceptualization, W.Z., M.M., and S.S.; software, writing—original draft preparation, W.Z. and M.M.; writing—review and editing, W.Z., M.M., and S.S.; graphic materials, S. S, W.Z., and M.M.; funding acquisitions, W.Z. and S.S. All authors have read and agreed to the published version of the manuscript.

**Funding:** This research was funded partially by the Polish Ministry of Science and Higher Education, grant number for the Faculty of Chemistry of Wroclaw University of Science and Technology 8211104160/K19W03D10, and by the U.S. National Science Foundation under Grant No. 1954310.

**Data Availability Statement:** No new data were created or analyzed in this study. Data sharing is not applicable to this article.

**Acknowledgments:** A generous grant of computer time from the Wroclaw Supercomputer and Networking Center is acknowledged.

**Conflicts of Interest:** The authors declare no conflict of interest.

## References

1. Clark, T.; Hennemann, M.; Murray, J.S.; Politzer, P. Halogen bonding: The  $\sigma$ -hole: Proceedings of “Modeling interactions in biomolecules II”, Prague, September 5th–9th, 2005. *J. Mol. Model.* **2007**, *13*, 291–296. [[CrossRef](#)]
2. Guthrie, F. On the Iodide of Iodammonium. *J. Chem. Soc.* **1863**, *16*, 239–244. [[CrossRef](#)]
3. Remsen, I.; Norris, J.F. Action of the halogens on the methyl-amines. *Am. Chem. J.* **1896**, *18*, 90–96.
4. Hope, H.; McCullough, J.D. The crystal structure of the molecular complex of iodine with tetrahydroselenophene, C<sub>4</sub>H<sub>8</sub>Se.I<sub>2</sub>. *Acta Cryst.* **1964**, *17*, 712–718. [[CrossRef](#)]
5. Olie, K.; Mijlhoff, F.C. The crystal structure of POBr<sub>3</sub> and intermolecular bonding. *Acta Cryst. Sect. B* **1969**, *25*, 974–977. [[CrossRef](#)]

6. Brinck, T.; Murray, J.S.; Politzer, P. Surface electrostatic potentials of halogenated methanes as indicators of directional intermolecular interactions. *Int. J. Quantum Chem.* **1992**, *44*, 57–64. [[CrossRef](#)]
7. Murray, J.S.; Lane, P.; Clark, T.; Politzer, P. Sigma-hole bonding: Molecules containing group VI atoms. *J. Mol. Model.* **2007**, *13*, 1033–1038. [[CrossRef](#)]
8. Politzer, P.; Lane, P.; Concha, M.C.; Ma, Y.G.; Murray, J.S. An overview of halogen bonding. *J. Mol. Model.* **2007**, *13*, 305–311. [[CrossRef](#)] [[PubMed](#)]
9. Politzer, P.; Murray, J.S.; Concha, M.C. Sigma-hole bonding between like atoms; a fallacy of atomic charges. *J. Mol. Model.* **2008**, *14*, 659–665. [[CrossRef](#)] [[PubMed](#)]
10. Murray, J.S.; Lane, P.; Politzer, P. Expansion of the sigma-hole concept. *J. Mol. Model.* **2009**, *15*, 723–729. [[CrossRef](#)] [[PubMed](#)]
11. Politzer, P.; Murray, J.S.; Clark, T. Halogen bonding: An electrostatically-driven highly directional noncovalent interaction. *Phys. Chem. Chem. Phys.* **2010**, *12*, 7748–7757. [[CrossRef](#)] [[PubMed](#)]
12. Murray, J.S.; Politzer, P. The electrostatic potential: An overview. *Wires Comput. Mol. Sci.* **2011**, *1*, 153–163. [[CrossRef](#)]
13. Murray, J.S.; Politzer, P. Interaction and polarization energy relationships in  $\sigma$ -hole and  $\pi$ -hole bonding. *Crystals* **2020**, *10*, 76. [[CrossRef](#)]
14. Politzer, P.; Murray, J.S. Halogen Bonding: An Interim Discussion. *ChemPhysChem* **2013**, *14*, 278–294. [[CrossRef](#)] [[PubMed](#)]
15. Politzer, P.; Murray, J.S.; Clark, T. sigma-Hole Bonding: A Physical Interpretation. *Top. Curr. Chem.* **2015**, *358*, 19–42. [[PubMed](#)]
16. Politzer, P.; Murray, J.S.; Clark, T.; Resnati, G. The sigma-hole revisited. *Phys. Chem. Chem. Phys.* **2017**, *19*, 32166–32178. [[CrossRef](#)]
17. Politzer, P.; Murray, J.S. Electrostatics and Polarization in sigma- and pi-Hole Noncovalent Interactions: An Overview. *ChemPhysChem* **2020**, *21*, 579–588. [[CrossRef](#)]
18. Azofra, L.M.; Alkorta, I.; Scheiner, S. Chalcogen bonds in complexes of SOXY (X, Y = F, Cl) with nitrogen bases. *J. Phys. Chem. A* **2015**, *119*, 535–541. [[CrossRef](#)]
19. Vincent De Paul, N.N.; Scheiner, S. Chalcogen bonding between tetravalent SF<sub>4</sub> and amines. *J. Phys. Chem. A* **2014**, *118*, 10849–10856.
20. Alikhani, E.; Fuster, F.; Madebene, B.; Grabowski, S.J. Topological reaction sites-very strong chalcogen bonds. *Phys. Chem. Chem. Phys.* **2014**, *16*, 2430–2442. [[CrossRef](#)]
21. Wang, W.; Ji, B.; Zhang, Y. Chalcogen bond: A sister noncovalent bond to halogen bond. *J. Phys. Chem. A* **2009**, *113*, 8132–8135. [[CrossRef](#)]
22. de Azevedo Santos, L.; Ramalho, T.C.; Hamlin, T.A.; Bickelhaupt, F.M. Chalcogen bonds: Hierarchical ab initio benchmark and density functional theory performance study. *J. Comput. Chem.* **2021**, *42*, 688–698. [[CrossRef](#)]
23. de Azevedo Santos, L.; van der Lubbe, S.C.C.; Hamlin, T.A.; Ramalho, T.C.; Matthias Bickelhaupt, F. A Quantitative Molecular Orbital Perspective of the Chalcogen Bond. *ChemistryOpen* **2021**. [[CrossRef](#)]
24. Alkorta, I.; Elguero, J.; Del Bene, J.E. Pnictogen Bonded Complexes of PO<sub>2</sub>X (X = F, Cl) with Nitrogen Bases. *J. Phys. Chem. A* **2013**, *117*, 10497–10503. [[CrossRef](#)] [[PubMed](#)]
25. Del Bene, J.E.; Alkorta, I.; Elguero, J. Properties of Complexes H<sub>2</sub>C=(X)P:PXH<sub>2</sub>, for X = F, Cl, OH, CN, NC, CCH, H, CH<sub>3</sub>, and BH<sub>2</sub>: P center dot center dot center dot P Pnictogen Bonding at sigma-Holes and pi-Holes. *J. Phys. Chem. A* **2013**, *117*, 11592–11604. [[CrossRef](#)]
26. Scheiner, S. Detailed comparison of the pnictogen bond with chalcogen, halogen, and hydrogen bonds. *Int. J. Quantum Chem.* **2013**, *113*, 1609–1620. [[CrossRef](#)]
27. Scheiner, S. The pnictogen bond: Its relation to hydrogen, halogen, and other noncovalent bonds. *Acc. Chem. Res.* **2013**, *46*, 280–288. [[CrossRef](#)] [[PubMed](#)]
28. Guan, L.Y.; Mo, Y.R. Electron Transfer in Pnictogen Bonds. *J. Phys. Chem. A* **2014**, *118*, 8911–8921. [[CrossRef](#)] [[PubMed](#)]
29. Bauza, A.; Mooibroek, T.J.; Frontera, A. Tetrel-Bonding Interaction: Rediscovered Supramolecular Force? *Angew. Chem. Int. Ed.* **2013**, *52*, 12317–12321. [[CrossRef](#)] [[PubMed](#)]
30. Bauza, A.; Mooibroek, T.J.; Frontera, A. Tetrel Bonding Interactions. *Chem. Rec.* **2016**, *16*, 473–487. [[CrossRef](#)]
31. Marin-Luna, M.; Alkorta, I.; Elguero, J. Cooperativity in Tetrel Bonds. *J. Phys. Chem. A* **2016**, *120*, 648–656. [[CrossRef](#)] [[PubMed](#)]
32. Desiraju, G.R.; Shing Ho, P.; Kloo, L.; Legon, A.C.; Marquardt, R.; Metrangolo, P.; Politzer, P.; Resnati, G.; Rissanen, K. Definition of the halogen bond (IUPAC recommendations 2013). *Pure Appl. Chem.* **2013**, *85*, 1711–1713. [[CrossRef](#)]
33. Aakeroy, C.B.; Bryce, D.L.; Desiraju, G.; Frontera, A.; Legon, A.C.; Nicotra, F.; Rissanen, K.; Scheiner, S.; Terraneo, G.; Metrangolo, P.; et al. Definition of the chalcogen bond (IUPAC Recommendations 2019). *Pure Appl. Chem.* **2019**, *91*, 1889–1892. [[CrossRef](#)]
34. Mahmoudi, G.; Afkhami, F.A.; Zangrando, E.; Kaminsky, W.; Frontera, A.; Safin, D.A. A supramolecular 3D structure constructed from a new metal chelate self-assembled from Sn(NCS)<sub>2</sub> and phenyl(pyridin-2-yl)methylenepicolinohydrazide. *J. Mol. Struct.* **2021**, *1224*, 129188. [[CrossRef](#)]
35. Zhang, J.H.; Su, Z.Z.; Luo, J.X.; Zhao, Y.; Wang, H.G.; Ying, S.M. Synthesis, structure, and characterization of a mixed amines thiogermanate [NH<sub>4</sub>]<sub>2</sub>[NH<sub>2</sub>(CH<sub>3</sub>)<sub>2</sub>]<sub>2</sub>(2)Ge<sub>2</sub>S<sub>6</sub>. *Polyhedron* **2020**, *182*, 114486. [[CrossRef](#)]
36. Zelenkov, L.E.; Ivanov, D.M.; Sadykov, E.K.; Bokach, N.A.; Galmes, B.; Frontera, A.; Kukushkin, V.Y. Semicoordination Bond Breaking and Halogen Bond Making Change the Supramolecular Architecture of Metal-Containing Aggregates. *Cryst. Growth Des.* **2020**, *20*, 6956–6965. [[CrossRef](#)]

37. Yusof, E.N.M.; Latif, M.A.M.; Tahir, M.I.M.; Sakoff, J.A.; Veerakumarasivam, A.; Page, A.J.; Tiekink, E.R.T.; Ravoof, T.B.S.A. Homoleptic tin(IV) compounds containing tridentate ONS dithiocarbazate Schiff bases: Synthesis, X-ray crystallography, DFT and cytotoxicity studies. *J. Mol. Struct.* **2020**, *1205*, 127635. [[CrossRef](#)]
38. Walton, I.; Chen, C.; Rimsza, J.M.; Nenoff, T.M.; Walton, K.S. Enhanced Sulfur Dioxide Adsorption in UiO-66 Through Crystal Engineering and Chalcogen Bonding. *Cryst. Growth Des.* **2020**, *20*, 6139–6146. [[CrossRef](#)]
39. Venosova, B.; Koziskova, J.; Kozisek, J.; Herich, P.; Luspai, K.; Petricek, V.; Hartung, J.; Muller, M.; Hubschle, C.B.; van Smaalen, S.; et al. Charge density of 4-methyl-3-[(tetrahydro-2H-pyran-2-yl)oxy]thiazole-2(3H)-thione. A comprehensive multipole refinement, maximum entropy method and density functional theory study. *Acta Cryst. B* **2020**, *76*, 450–468. [[CrossRef](#)]
40. Villasenor-Granados, T.O.; Montes-Tolentino, P.; Rodriguez-Lopez, G.; Sanchez-Ruiz, S.A.; Flores-Parra, A. Structural analysis of tris(5-methyl-[1,3,5]-dithiazinan-2-yl)stibine, its reactions with chalcogens. Intramolecular chalcogen-bonding interactions. *J. Mol. Struct.* **2020**, *1200*, 127050. [[CrossRef](#)]
41. Kumar, V.; Xu, Y.J.; Bryce, D.L. Double Chalcogen Bonds: Crystal Engineering Stratagems via Diffraction and Multinuclear Solid-State Magnetic Resonance Spectroscopy. *Chem. Eur. J.* **2020**, *26*, 3275–3286. [[CrossRef](#)]
42. Fourmigue, M.; Dhaka, A. Chalcogen bonding in crystalline diselenides and selenocyanates: From molecules of pharmaceutical interest to conducting materials. *Coord. Chem. Rev.* **2020**, *403*, 213084. [[CrossRef](#)]
43. Michalczyk, M.; Malik, M.; Zierkiewicz, W.; Scheiner, S. Experimental and Theoretical Studies of Dimers Stabilized by Two Chalcogen Bonds in the Presence of a N...N Pnictogen Bond. *J. Phys. Chem. A* **2021**, *125*, 657–668. [[CrossRef](#)] [[PubMed](#)]
44. Kinzhalov, M.A.; Popova, E.A.; Petrov, M.L.; Khoroshilova, O.V.; Mahmudov, K.T.; Pombeiro, A.J.L. Pnictogen and chalcogen bonds in cyclometalated iridium(III) complexes. *Inorg. Chim. Acta* **2018**, *477*, 31–33. [[CrossRef](#)]
45. Zapata, F.; Gonzalez, L.; Bastida, A.; Bautista, D.; Caballero, A. Formation of self-assembled supramolecular polymers by anti-electrostatic anion-anion and halogen bonding interactions. *Chem. Commun.* **2020**, *56*, 7084–7087. [[CrossRef](#)] [[PubMed](#)]
46. Soldatova, N.S.; Postnikov, P.S.; Suslonov, V.V.; Kissler, T.Y.; Ivanov, D.M.; Yusubov, M.S.; Galmes, B.; Frontera, A.; Kukushkin, V.Y. Diaryliodonium as a double sigma-hole donor: The dichotomy of thiocyanate halogen bonding provides divergent solid state arylation by diaryliodonium cations. *Org. Chem. Front.* **2020**, *7*, 2230–2242. [[CrossRef](#)]
47. Scilabra, P.; Terraneo, G.; Daolio, A.; Baggioli, A.; Famulari, A.; Leroy, C.; Bryce, D.L.; Resnati, G. 4,4'-Dipyridyl Dioxide center dot SbF<sub>3</sub> Cocrystal: Pnictogen Bond Prevails over Halogen and Hydrogen Bonds in Driving Self-Assembly. *Cryst. Growth Des.* **2020**, *20*, 916–922. [[CrossRef](#)]
48. Nascimento, M.A.; Heyer, E.; Less, R.J.; Pask, C.M.; Arauzo, A.; Campo, J.; Rawson, J.M. An Investigation of Halogen Bonding as a Structure-Directing Interaction in Dithiadiazolyl Radicals. *Cryst. Growth Des.* **2020**, *20*, 4313–4324. [[CrossRef](#)]
49. Pramanik, S.; Chopra, D. Unravelling the Importance of H bonds,  $\sigma$ -hole and  $\pi$ -hole-Directed Intermolecular Interactions in Nature. *J. Indian I Sci.* **2020**, *100*, 43–59. [[CrossRef](#)]
50. Orlova, A.P.; Jasien, P.G. Halogen bonding in self-assembling systems: A comparison of intra- and interchain binding energies. *Comput. Chem.* **2018**, *1139*, 63–69. [[CrossRef](#)]
51. Tiekink, E.R.T. A Survey of Supramolecular Aggregation Based on Main Group Element Selenium Secondary Bonding Interactions—A Survey of the Crystallographic Literature. *Crystals* **2020**, *10*, 503. [[CrossRef](#)]
52. Seth, S.K.; Bauzá, A.; Frontera, A. Chapter 9 Quantitative Analysis of Weak Non-covalent  $\sigma$ -Hole and  $\pi$ -Hole Interactions. In *Monogr Supramol Chem*; The Royal Society of Chemistry: London, UK, 2019; pp. 285–333.
53. Taylor, M.S. Anion recognition based on halogen, chalcogen, pnictogen and tetrel bonding. *Coord. Chem. Rev.* **2020**, *413*, 213270. [[CrossRef](#)]
54. Navarro-Garcia, E.; Galmes, B.; Velasco, M.D.; Frontera, A.; Caballero, A. Anion Recognition by Neutral Chalcogen Bonding Receptors: Experimental and Theoretical Investigations. *Chem. Eur. J.* **2020**, *26*, 4706–4713. [[CrossRef](#)] [[PubMed](#)]
55. Borissov, A.; Marques, I.; Lim, J.Y.C.; Felix, V.; Smith, M.D.; Beer, P.D. Anion Recognition in Water by Charge-Neutral Halogen and Chalcogen Bonding Foldamer Receptors. *J. Am. Chem. Soc.* **2019**, *141*, 4119–4129. [[CrossRef](#)] [[PubMed](#)]
56. Semenov, N.A.; Gorbunov, D.E.; Shakhova, M.V.; Salnikov, G.E.; Bagryanskaya, I.Y.; Korolev, V.V.; Beckmann, J.; Gritsan, N.P.; Zibarev, A.V. Donor-Acceptor Complexes between 1,2,5-Chalcogenadiazoles (Te, Se, S) and the Pseudohalides CN<sup>-</sup> and XCN<sup>-</sup> (X = O, S, Se, Te). *Chem. Eur. J.* **2018**, *24*, 12983–12991. [[CrossRef](#)]
57. Naseer, M.M.; Hussain, M.; Bauza, A.; Lo, K.M.; Frontera, A. Intramolecular Noncovalent Carbon Bonding Interaction Stabilizes the cis Conformation in Acylhydrazones. *Chempluschem* **2018**, *83*, 881–885. [[CrossRef](#)] [[PubMed](#)]
58. Lim, J.Y.C.; Beer, P.D. Sigma-Hole Interactions in Anion Recognition. *Chem-US* **2018**, *4*, 731–783. [[CrossRef](#)]
59. Liu, Y.-Z.; Yuan, K.; Liu, L.; Yuan, Z.; Zhu, Y.-C. Anion Recognition Based on a Combination of Double-Dentate Hydrogen Bond and Double-Side Anion- $\pi$  Noncovalent Interactions. *J. Phys. Chem. A* **2017**, *121*, 892–900. [[CrossRef](#)]
60. Lim, J.Y.C.; Marques, I.; Thompson, A.L.; Christensen, K.E.; Felix, V.; Beer, P.D. Chalcogen Bonding Macrocycles and [2]Rotaxanes for Anion Recognition. *J. Am. Chem. Soc.* **2017**, *139*, 3122–3133. [[CrossRef](#)]
61. Scheiner, S. Tetrel Bonding as a Vehicle for Strong and Selective Anion Binding. *Molecules* **2018**, *23*, 1147. [[CrossRef](#)]
62. Kociok-Kohn, G.; Mahon, M.F.; Molloy, K.C.; Price, G.J.; Prior, T.J.; Smith, D.R.G. Biomimetic polyorganosiloxanes: Model compounds for new materials. *Dalton Trans.* **2014**, *43*, 7734–7746. [[CrossRef](#)] [[PubMed](#)]
63. Politzer, P.; Murray, J.S.; Concha, M.C. Halogen bonding and the design of new materials: Organic bromides, chlorides and perhaps even fluorides as donors. *J. Mol. Model.* **2007**, *13*, 643–650. [[CrossRef](#)] [[PubMed](#)]

64. Radovic, L.R. Probing the ‘elephant’: On the essential difference between graphenes and polycyclic aromatic hydrocarbons. *Carbon* **2021**, *171*, 798–805. [[CrossRef](#)]
65. Maruthapandi, M.; Eswaran, L.; Cohen, R.; Perkas, N.; Luong, J.H.T.; Gedanken, A. Silica-Supported Nitrogen-Enriched Porous Benzimidazole-Linked and Triazine-Based Polymers for the Adsorption of CO<sub>2</sub>. *Langmuir* **2020**, *36*, 4280–4288. [[CrossRef](#)] [[PubMed](#)]
66. Kar, I.; Chatterjee, J.; Harnagea, L.; Kushnirenko, Y.; Fedorov, A.V.; Shrivastava, D.; Buchner, B.; Mahadevan, P.; Thirupathiah, S. Metal-chalcogen bond-length induced electronic phase transition from semiconductor to topological semimetal in ZrX<sub>2</sub> (X = Se and Te). *Phys. Rev. B* **2020**, *101*, 165122. [[CrossRef](#)]
67. Isaeva, A.; Ruck, M. Crystal Chemistry and Bonding Patterns of Bismuth-Based Topological Insulators. *Inorg. Chem.* **2020**, *59*, 3437–3451. [[CrossRef](#)] [[PubMed](#)]
68. Ho, P.C.; Wang, J.Z.; Meloni, F.; Vargas-Baca, I. Chalcogen bonding in materials chemistry. *Coord. Chem. Rev.* **2020**, *422*, 213464. [[CrossRef](#)]
69. Daniels, C.L.; Knobeloch, M.; Yox, P.; Adamson, M.A.S.; Chen, Y.H.; Dorn, R.W.; Wu, H.; Zhou, G.Q.; Fan, H.J.; Rossini, A.J.; et al. Intermetallic Nanocatalysts from Heterobimetallic Group 10–14 Pyridine-2-thiolate Precursors. *Organometallics* **2020**, *39*, 1092–1104. [[CrossRef](#)]
70. Zhang, Y.; Wang, W.Z.; Wang, Y.B. Tetrel bonding on graphene. *Comput. Chem.* **2019**, *1147*, 8–12. [[CrossRef](#)]
71. Sung, S.H.; Schnitzer, N.; Brown, L.; Park, J.; Hovden, R. Stacking, strain, and twist in 2D materials quantified by 3D electron diffraction. *Phys. Rev. Mater.* **2019**, *3*, 064003. [[CrossRef](#)]
72. Mahmudov, K.T.; Kopylovich, M.N.; Guedes da Silva, M.F.C.; Pombeiro, A.J.L. Chalcogen bonding in synthesis, catalysis and design of materials. *Dalton Trans.* **2017**, *46*, 10121–10138. [[CrossRef](#)]
73. Pina, M.D.N.; Frontera, A.; Bauza, A. Quantifying Intramolecular Halogen Bonds in Nucleic Acids: A Combined Protein Data Bank and Theoretical Study. *Acs Chem. Biol.* **2020**, *15*, 1942–1948. [[CrossRef](#)]
74. Lundemba, A.S.; Bibelayi, D.D.; Wood, P.A.; Pradon, J.; Yav, Z.G. sigma-Hole interactions in small-molecule compounds containing divalent sulfur groups R-1-S-R-2. *Acta Cryst. B* **2020**, *76*, 707–718. [[CrossRef](#)] [[PubMed](#)]
75. Scheiner, S. Differential Binding of Tetrel-Bonding Bipodal Receptors to Monatomic and Polyatomic Anions. *Molecules* **2019**, *24*, 227. [[CrossRef](#)] [[PubMed](#)]
76. Riel, A.M.S.; Huynh, H.T.; Jeannin, O.; Berryman, O.; Fourmigue, M. Organic Selenocyanates as Halide Receptors: From Chelation to One-Dimensional Systems. *Cryst. Growth Des.* **2019**, *19*, 1418–1425. [[CrossRef](#)]
77. Michalczyk, M.; Zierkiewicz, W.; Wysokinski, R.; Scheiner, S. Theoretical Studies of IR and NMR Spectral Changes Induced by Sigma-Hole Hydrogen, Halogen, Chalcogen, Pnicogen, and Tetrel Bonds in a Model Protein Environment. *Molecules* **2019**, *24*, 3329. [[CrossRef](#)]
78. Wei, Y.; Li, Q.; Scheiner, S. The pi-Tetrel Bond and its Influence on Hydrogen Bonding and Proton Transfer. *Chemphyschem* **2018**, *19*, 736–743. [[CrossRef](#)]
79. Trievel, R.C.; Scheiner, S. Crystallographic and Computational Characterization of Methyl Tetrel Bonding in S-Adenosylmethionine-Dependent Methyltransferases. *Molecules* **2018**, *23*, 2965. [[CrossRef](#)]
80. Scheiner, S. Halogen Bonds Formed between Substituted Imidazoliums and N Bases of Varying N-Hybridization. *Molecules* **2017**, *22*, 1634. [[CrossRef](#)]
81. Montaña, Á.M. The  $\sigma$  and  $\pi$  Holes. The Halogen and Tetrel Bondings: Their Nature, Importance and Chemical, Biological and Medicinal Implications. *Chemistryselect* **2017**, *2*, 9094–9112. [[CrossRef](#)]
82. Grabowski, S.J. Tetrel bond-sigma-hole bond as a preliminary stage of the S(N)<sub>2</sub> reaction. *Phys. Chem. Chem. Phys.* **2014**, *16*, 1824–1834. [[CrossRef](#)]
83. Angarov, V.; Kozuch, S. On the  $\sigma$ ,  $\pi$  and  $\delta$  hole interactions: A molecular orbital overview. *New J. Chem.* **2018**, *42*, 1413–1422. [[CrossRef](#)]
84. Bauza, A.; Mooibroek, T.J.; Frontera, A. The Bright Future of Unconventional sigma/-Hole Interactions. *Chemphyschem* **2015**, *16*, 2496–2517. [[CrossRef](#)]
85. Gao, L.; Zeng, Y.; Zhang, X.; Meng, L. Comparative studies on group III sigma-hole and pi-hole interactions. *J. Comput. Chem.* **2016**, *37*, 1321–1327. [[CrossRef](#)] [[PubMed](#)]
86. Bauza, A.; Mooibroek, T.J.; Frontera, A. Directionality of pi-holes in nitro compounds. *Chem. Commun.* **2015**, *51*, 1491–1493. [[CrossRef](#)] [[PubMed](#)]
87. Murray, J.S.; Lane, P.; Clark, T.; Riley, K.E.; Politzer, P. sigma-Holes, pi-holes and electrostatically-driven interactions. *J. Mol. Model.* **2012**, *18*, 541–548. [[CrossRef](#)] [[PubMed](#)]
88. Grabowski, S.J. The Nature of Trel Bonds, a Case of B and Al Centres Bonded with Electron Rich Sites. *Molecules* **2020**, *25*, 2703. [[CrossRef](#)]
89. Grabowski, S.J. Trel bond and coordination of triel centres-Comparison with hydrogen bond interaction. *Coord. Chem. Rev.* **2020**, *407*, 213171. [[CrossRef](#)]
90. Xu, Z.F.; Li, Y. Trel bonds in RZH(2)center dot center dot center dot NH<sub>3</sub>: Hybridization, solvation, and substitution. *J. Mol. Model.* **2019**, *25*, 219. [[CrossRef](#)]
91. Jablonski, M. Hydride-Triel Bonds. *J. Comput. Chem.* **2018**, *39*, 1177–1191. [[CrossRef](#)]
92. Grabowski, S.J. Two faces of triel bonds in boron trihalide complexes. *J. Comput. Chem.* **2018**, *39*, 472–480. [[CrossRef](#)]

93. Esrafil, M.D.; Mousavian, P. The triel bond: A potential force for tuning anion- $\pi$  interactions. *Mol. Phys.* **2018**, *116*, 388–398. [[CrossRef](#)]
94. Grabowski, S.J. Triel bonds-complexes of boron and aluminum trihalides and trihydrides with benzene. *Struct. Chem.* **2017**, *28*, 1163–1171. [[CrossRef](#)]
95. Grabowski, S.J.  $\pi$ -Hole Bonds: Boron and Aluminum Lewis Acid Centers. *Chemphyschem* **2015**, *16*, 1470–1479. [[CrossRef](#)] [[PubMed](#)]
96. Burgi, H.B.; Dunitz, J.D.; Shefter, E. Geometrical reaction coordinates. II. Nucleophilic addition to a carbonyl group. *J. Am. Chem. Soc.* **1973**, *95*, 5065–5067. [[CrossRef](#)]
97. Harder, M.; Kuhn, B.; Diederich, F. Efficient Stacking on Protein Amide Fragments. *Chemmedchem* **2013**, *8*, 397–404. [[CrossRef](#)]
98. Bartlett, G.J.; Choudhary, A.; Raines, R.T.; Woolfson, D.N.  $n \rightarrow \pi^*$  interactions in proteins. *Nat. Chem. Biol.* **2010**, *6*, 615–620. [[CrossRef](#)]
99. Andleeb, H.; Khan, I.; Bauza, A.; Tahir, M.N.; Simpson, J.; Hameed, S.; Frontera, A. Synthesis and supramolecular self-assembly of thioxothiazolidinone derivatives driven by  $\pi$ -bonding and diverse 7 hole interactions: A combined experimental and theoretical analysis. *J. Mol. Struct.* **2017**, *1139*, 209–221. [[CrossRef](#)]
100. Gomila, R.M.; Frontera, A. Covalent and Non-covalent Noble Gas Bonding Interactions in XeFn Derivatives ( $n = 2-6$ ): A Combined Theoretical and ICSD Analysis. *Front. Chem.* **2020**, *8*, 395. [[CrossRef](#)]
101. Bauza, A.; Frontera, A.  $\sigma/\pi$ -Hole noble gas bonding interactions: Insights from theory and experiment. *Coord. Chem. Rev.* **2019**, *404*, 213112. [[CrossRef](#)]
102. Esrafil, M.D.; Vessally, E. The strengthening effect of a hydrogen or lithium bond on the  $Z \cdots N$  aerogen bond ( $Z = \text{Ar, Kr and Xe}$ ): A comparative study. *Mol. Phys.* **2016**, *114*, 3265–3276. [[CrossRef](#)]
103. Bauza, A.; Frontera, A.  $\pi$ -Hole aerogen bonding interactions. *Phys. Chem. Chem. Phys.* **2015**, *17*, 24748–24753. [[CrossRef](#)] [[PubMed](#)]
104. Bauzá, A.; Frontera, A. Aerogen Bonding Interaction: A New Supramolecular Force? *Angew. Chem. Int. Ed.* **2015**, *54*, 7340–7343. [[CrossRef](#)] [[PubMed](#)]
105. Alkorta, I.; Elguero, J.; Frontera, A. Not Only Hydrogen Bonds: Other Noncovalent Interactions. *Crystals* **2020**, *10*, 180. [[CrossRef](#)]
106. Hou, M.C.; Zhu, Y.F.; Li, Q.Z.; Scheiner, S. Tuning the Competition between Hydrogen and Tetrel Bonds by a Magnesium Bond. *Chemphyschem* **2020**, *21*, 212–219. [[CrossRef](#)]
107. Alkorta, I.; Legon, A.C. Non-Covalent Interactions Involving Alkaline-Earth Atoms and Lewis Bases B: An ab Initio Investigation of Beryllium and Magnesium Bonds, B center dot center dot center dot MR2 ( $M = \text{Be or Mg}$ , and  $R = \text{H, F or CH}_3$ ). *Inorganics* **2019**, *7*, 35. [[CrossRef](#)]
108. Grabowski, S.J. Magnesium Bonds: From Divalent Mg Centres to Trigonal and Tetrahedral Coordination. *Chemistryselect* **2018**, *3*, 3147–3154. [[CrossRef](#)]
109. Alikhani, M.E. Beryllium bonding: Insights from the  $\sigma$ - and  $\pi$ -hole analysis. *J. Mol. Model.* **2020**, *26*, 94. [[CrossRef](#)]
110. Zhang, Z.; Lu, T.; Ding, L.Y.; Wang, G.Y.; Wang, Z.X.; Zheng, B.S.; Liu, Y.; Ding, X.L. Cooperativity effects between regium-bonding and pnicogen-bonding interactions in ternary MF center dot center dot center dot PH3O center dot center dot center dot MF ( $M = \text{Cu, Ag, Au}$ ): An ab initio study. *Mol. Phys.* **2020**, *118*, e1784478. [[CrossRef](#)]
111. Wang, R.J.; Wang, Z.; Yu, X.F.; Li, Q.Z. Synergistic and Diminutive Effects between Regium and Aerogen Bonds. *Chemphyschem* **2020**, *21*, 2426–2431. [[CrossRef](#)] [[PubMed](#)]
112. Sanchez-Sanz, G.; Trujillo, C.; Alkorta, I.; Elguero, J. Rivalry between Regium and Hydrogen Bonds Established within Diatomic Coinage Molecules and Lewis Acids/Bases. *Chemphyschem* **2020**, *21*, 2557–2563. [[CrossRef](#)]
113. Alkorta, I.; Trujillo, C.; Sanchez-Sanz, G.; Elguero, J. Regium Bonds between Silver(I) Pyrazolates Dinuclear Complexes and Lewis Bases ( $\text{N}_2$ ,  $\text{OH}_2$ ,  $\text{NCH}$ ,  $\text{SH}_2$ ,  $\text{NH}_3$ ,  $\text{PH}_3$ ,  $\text{CO}$  and  $\text{CNH}$ ). *Crystals* **2020**, *10*, 137. [[CrossRef](#)]
114. Sanchez-Sanz, G.; Trujillo, C.; Alkorta, I.; Elguero, J. Understanding Regium Bonds and their Competition with Hydrogen Bonds in  $\text{Au-2:HX}$  Complexes. *Chemphyschem* **2019**, *20*, 1572–1580. [[CrossRef](#)]
115. Zierkiewicz, W.; Michalczyk, M.; Scheiner, S. Regium bonds between Mn clusters ( $M = \text{Cu, Ag, Au}$  and  $n = 2-6$ ) and nucleophiles  $\text{NH}_3$  and  $\text{HCN}$ . *Phys. Chem. Chem. Phys.* **2018**, *20*, 22498–22509. [[CrossRef](#)] [[PubMed](#)]
116. Xia, T.; Li, D.; Cheng, L.J. Theoretical analysis of the spodium bonds in  $\text{HgCl}_2$  center dot center dot center dot L ( $L = \text{ClR, SR}_2$ , and  $\text{PR}_3$ ) dimers. *Chem. Phys.* **2020**, *539*, 110978. [[CrossRef](#)]
117. Mahmoudi, G.; Masoudiasl, A.; Babashkina, M.G.; Frontera, A.; Doert, T.; White, J.M.; Zangrando, E.; Zubkov, F.I.; Safin, D.A. On the importance of  $\pi$ -hole spodium bonding in tricoordinated Hg-II complexes. *Dalton T* **2020**, *49*, 17547–17551. [[CrossRef](#)] [[PubMed](#)]
118. Mahmoudi, G.; Lawrence, S.E.; Cisterna, J.; Cardenas, A.; Brito, I.; Frontera, A.; Safin, D.A. A new spodium bond driven coordination polymer constructed from mercury(II) azide and 1,2-bis(pyridin-2-ylmethylene)hydrazine. *New J. Chem.* **2020**, *44*, 21100–21107. [[CrossRef](#)]
119. Bauze, A.; Alkorta, I.; Elguero, J.; Mooibroek, T.J.; Frontera, A. Spodium Bonds: Noncovalent Interactions Involving Group 12 Elements. *Angew. Chem. Int. Ed.* **2020**, *59*, 17482–17487. [[CrossRef](#)]
120. Frontera, A.  $\sigma$ - and  $\pi$ -Hole Interactions. *Crystals* **2020**, *10*, 721. [[CrossRef](#)]
121. Cavallo, G.; Metrangolo, P.; Milani, R.; Pilati, T.; Priimagi, A.; Resnati, G.; Terraneo, G. The halogen bond. *Chem. Rev.* **2016**, *116*, 2478–2601. [[CrossRef](#)] [[PubMed](#)]

122. Esrafil, M.D.; Mohammadirad, N. An ab initio study on tunability of  $\sigma$ -hole interactions in XHS:PH<sub>2</sub>Y and XH<sub>2</sub>P:SHY complexes (X = F, Cl, Br; Y = H, OH, OCH<sub>3</sub>, CH<sub>3</sub>, C<sub>2</sub>H<sub>5</sub>, and NH<sub>2</sub>). *J. Mol. Model.* **2015**, *21*, 2727. [CrossRef]
123. Riley, K.E.; Murray, J.S.; Fanfrlik, J.; Rezac, J.; Sola, R.J.; Concha, M.C.; Ramos, F.M.; Politzer, P. Halogen bond tunability II: The varying roles of electrostatic and dispersion contributions to attraction in halogen bonds. *J. Mol. Model.* **2013**, *19*, 4651–4659. [CrossRef]
124. Riley, K.E.; Murray, J.S.; Fanfrlik, J.; Rezac, J.; Sola, R.J.; Concha, M.C.; Ramos, F.M.; Politzer, P. Halogen bond tunability I: The effects of aromatic fluorine substitution on the strengths of halogen-bonding interactions involving chlorine, bromine, and iodine. *J. Mol. Model.* **2011**, *17*, 3309–3318. [CrossRef]
125. Politzer, P.; Murray, J.S. sigma-Hole Interactions: Perspectives and Misconceptions. *Crystals* **2017**, *7*, 212. [CrossRef]
126. Bulat, F.A.; Toro-Labbe, A.; Brinck, T.; Murray, J.S.; Politzer, P. Quantitative analysis of molecular surfaces: Areas, volumes, electrostatic potentials and average local ionization energies. *J. Mol. Model.* **2010**, *16*, 1679–1691. [CrossRef]
127. Murray, J.S.; Politzer, P. Molecular electrostatic potentials and noncovalent interactions. *Wires Comput. Mol. Sci.* **2017**, *7*, e13260. [CrossRef]
128. Politzer, P.; Murray, J.S. sigma-holes and pi-holes: Similarities and differences. *J. Comput. Chem.* **2018**, *39*, 464–471. [CrossRef]
129. Clark, T.; Murray, J.S.; Politzer, P. Role of Polarization in Halogen Bonds. *Aust. J. Chem.* **2014**, *67*, 451–456. [CrossRef]
130. Hennemann, M.; Murray, J.S.; Politzer, P.; Riley, K.E.; Clark, T. Polarization-induced sigma-holes and hydrogen bonding. *J. Mol. Model.* **2012**, *18*, 2461–2469. [CrossRef] [PubMed]
131. Riley, K.E.; Hobza, P. The relative roles of electrostatics and dispersion in the stabilization of halogen bonds. *Phys. Chem. Chem. Phys.* **2013**, *15*, 17742–17751. [CrossRef] [PubMed]
132. Zierkiewicz, W.; Michalczyk, M.; Scheiner, S. Aerogen bonds formed between AeOF(2) (Ae = Kr, Xe) and diazines: Comparisons between sigma-hole and pi-hole complexes. *Phys. Chem. Chem. Phys.* **2018**, *20*, 4676–4687. [CrossRef]
133. Zierkiewicz, W.; Michalczyk, M.; Wysokinski, R.; Scheiner, S. On the ability of pnictogen atoms to engage in both sigma and pi-hole complexes. Heterodimers of ZF<sub>2</sub>C<sub>6</sub>H<sub>5</sub> (Z = P, As, Sb, Bi) and NH<sub>3</sub>. *J. Mol. Model.* **2019**, *25*, 152. [CrossRef] [PubMed]
134. Wysokinski, R.; Zierkiewicz, W.; Michalczyk, M.; Scheiner, S. How Many Pnictogen Bonds can be Formed to a Central Atom Simultaneously? *J. Phys. Chem. A* **2020**, *124*, 2046–2056. [CrossRef] [PubMed]
135. Zierkiewicz, W.; Wysokinski, R.; Michalczyk, M.; Scheiner, S. Chalcogen bonding of two ligands to hypervalent YF<sub>4</sub> (Y = S, Se, Te, Po). *Phys. Chem. Chem. Phys.* **2019**, *21*, 20829–20839. [CrossRef] [PubMed]
136. Michalczyk, M.; Zierkiewicz, W.; Wysokinski, R.; Scheiner, S. Hexacoordinated Tetrel-Bonded Complexes between TF<sub>4</sub> (T = Si, Ge, Sn, Pb) and NCH: Competition between sigma- and pi-Holes. *Chemphyschem* **2019**, *20*, 959–966. [CrossRef]
137. Makarewicz, E.; Lundell, J.; Gordon, A.J.; Berski, S. On the nature of interactions in the F<sub>2</sub> OXe(...) NCCH<sub>3</sub> complex: Is there the Xe(IV)N bond? *J. Comput. Chem.* **2016**, *37*, 1876–1886. [CrossRef]
138. Brock, D.S.; Bilir, V.; Mercier, H.P.A.; Schrobilgen, G.J. XeOF<sub>2</sub>, F<sub>2</sub>OXeN equivalent to CCH<sub>3</sub>, and XeOF<sub>2</sub> center dot nHF: Rare examples of Xe(IV) oxide fluorides. *J. Am. Chem. Soc.* **2007**, *129*, 3598–3611. [CrossRef]
139. Brock, D.S.; de Pury, J.J.C.; Mercier, H.P.A.; Schrobilgen, G.J.; Silvi, B. A Rare Example of a Krypton Difluoride Coordination Compound: [BrOF<sub>2</sub>][AsF<sub>6</sub>]center dot 2KrF(2). *J. Am. Chem. Soc.* **2010**, *132*, 3533–3542. [CrossRef]
140. Wang, H.; Wang, W.; Jin, W.J.  $\sigma$ -Hole Bond vs  $\pi$ -Hole Bond: A Comparison Based on Halogen Bond. *Chem. Rev.* **2016**, *116*, 5072–5104. [CrossRef]
141. Zhang, Y.-H.; Li, Y.-L.; Yang, J.; Zhou, P.-P.; Xie, K. Noncovalent functionalization of graphene via  $\pi$ -hole $\cdots\pi$  and  $\sigma$ -hole $\cdots\pi$  interactions. *Struct. Chem.* **2020**, *31*, 97–101. [CrossRef]
142. Yang, F.-L.; Yang, X.; Wu, R.-Z.; Yan, C.-X.; Yang, F.; Ye, W.; Zhang, L.-W.; Zhou, P.-P. Intermolecular interactions between  $\sigma$ - and  $\pi$ -holes of bromopentafluorobenzene and pyridine: Computational and experimental investigations. *Phys. Chem. Chem. Phys.* **2018**, *20*, 11386–11395. [CrossRef] [PubMed]
143. Liu, Z.F.; Chen, X.; Wu, W.X.; Zhang, G.Q.; Li, X.; Li, Z.Z.; Jin, W.J. 1,3,5-Trifluoro-2,4,6-triiodobenzene: A neglected NIR phosphor with prolonged lifetime by  $\sigma$ -hole and  $\pi$ -hole capture. *Spectrochim. Acta Part A Mol. Biomol. Spectrosc.* **2020**, *224*, 117428. [CrossRef]
144. Shukla, R.; Khan, I.; Ibrar, A.; Simpson, J.; Chopra, D. Complex electronic interplay of  $\sigma$ -hole and  $\pi$ -hole interactions in crystals of halogen substituted 1,3,4-oxadiazol-2(3H)-thiones. *Crystengcomm* **2017**, *19*, 3485–3498. [CrossRef]
145. Li, L.; Wang, H.; Wang, W.; Jin, W.J. Interactions between haloperfluorobenzenes and fluoranthene in luminescent cocrystals from  $\pi$ -hole $\cdots\pi$  to  $\sigma$ -hole $\cdots\pi$  bonds. *Crystengcomm* **2017**, *19*, 5058–5067. [CrossRef]
146. Wang, J.; Mo, L.; Li, X.; Geng, Z.; Zeng, Y. The protonated 2-halogenated imidazolium cation as the noncovalent interaction donor: The  $\sigma$ -hole and  $\pi$ -hole interactions. *J. Mol. Model.* **2016**, *22*, 299. [CrossRef]
147. Zhang, Y.; Ji, B.M.; Tian, A.M.; Wang, W.Z. Communication: Competition between pi center dot center dot center dot pi interaction and halogen bond in solution: A combined C-13 NMR and density functional theory study. *J. Chem. Phys.* **2012**, *136*, 141101. [CrossRef] [PubMed]
148. Ma, N.; Zhang, Y.; Ji, B.M.; Tian, A.M.; Wang, W.Z. Structural Competition between Halogen Bonds and Lone-Pair center dot center dot center dot p Interactions in Solution. *Chemphyschem* **2012**, *13*, 1411–1414. [CrossRef] [PubMed]
149. Shukla, R.; Claiser, N.; Souhassou, M.; Lecomte, C.; Balkrishna, S.J.; Kumar, S.; Chopra, D. Exploring the simultaneous [sigma]-hole/[pi]-hole bonding characteristics of a Br...[pi] interaction in an ebselen derivative via experimental and theoretical electron-density analysis. *Iucrj* **2018**, *5*, 647–653. [CrossRef]

150. Lang, T.; Li, X.; Meng, L.; Zheng, S.; Zeng, Y. The cooperativity between the  $\sigma$ -hole and  $\pi$ -hole interactions in the  $\text{ClO}\cdots\text{XONO}_2/\text{XONO}\cdots\text{NH}_3$  ( $X = \text{Cl, Br, I}$ ) complexes. *Struct. Chem.* **2015**, *26*, 213–221. [[CrossRef](#)]
151. Solimannejad, M.; Nassirinia, N.; Amani, S. A computational study of 1:1 and 1:2 complexes of nitril halides ( $\text{O}_2\text{NX}$ ) with HCN and HNC. *Struct. Chem.* **2013**, *24*, 651–659. [[CrossRef](#)]
152. Solimannejad, M.; Ramezani, V.; Trujillo, C.; Alkorta, I.; Sanchez-Sanz, G.; Elguero, J. Competition and Interplay between sigma-Hole and pi-Hole Interactions: A Computational Study of 1:1 and 1:2 Complexes of Nitril Halides ( $\text{O}_2\text{NX}$ ) with Ammonia. *J. Phys. Chem. A* **2012**, *116*, 5199–5206. [[CrossRef](#)] [[PubMed](#)]
153. McDowell, S.A.C.; Joseph, J.A. A comparative study of model halogen-bonded,  $\pi$ -hole-bonded and cationic complexes involving  $\text{NCX AND H}_2\text{O}$  ( $X = \text{F, Cl, Br}$ ). *Mol. Phys.* **2015**, *113*, 16–21. [[CrossRef](#)]
154. Bauza, A.; Frontera, A. On the Versatility of  $\text{BH}_2\text{X}$  ( $X = \text{F, Cl, Br, and I}$ ) Compounds as Halogen-, Hydrogen-, and Trel-Bond Donors: An AbInitio Study. *Chemphyschem* **2016**, *17*, 3181–3186. [[CrossRef](#)] [[PubMed](#)]
155. Pal, R.; Nagendra, G.; Samarasimhareddy, M.; Sureshababu, V.V.; Guru Row, T.N. Observation of a reversible isomorphous phase transition and an interplay of “ $\sigma$ -holes” and “ $\pi$ -holes” in Fmoc-Leu- $\psi$ [CH<sub>2</sub>-NCS]. *Chem. Commun.* **2015**, *51*, 933–936. [[CrossRef](#)]
156. Dong, W.; Wang, Y.; Cheng, J.; Yang, X.; Li, Q. Competition between  $\sigma$ -hole pnicogen bond and  $\pi$ -hole tetrel bond in complexes of  $\text{CF}_2=\text{CFZH}_2$  ( $Z = \text{P, As, and Sb}$ ). *Mol. Phys.* **2019**, *117*, 251–259. [[CrossRef](#)]
157. Dong, W.; Yang, X.; Cheng, J.; Li, W.; Li, Q. Comparison for  $\sigma$ -hole and  $\pi$ -hole tetrel-bonded complexes involving  $\text{F}_2\text{CCFTF}_3$  (TC, Si, and Ge): Substitution, hybridization, and solvation effects. *J. Fluor. Chem.* **2018**, *207*, 38–44. [[CrossRef](#)]